Heliyon 10 (2024) e27454

Contents lists available at ScienceDirect

Heliyon

journal homepage: www.cell.com/heliyon

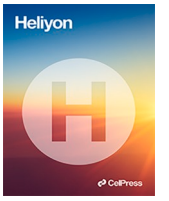

Research article

Preparation and thermal responsiveness of microencapsulated fluorinated liquids for automatic fire extinguishing

Hao Liu [a], Tianwei Zhang [a,d], Man Zhang [b,*], Cunwei Zhang [a,d], Zidong Guo [a,d], Yuhai Zhang [a], Haoran Chen [c], Yunchen Wu [d], Guiyun Zhang [d]

[a] Hebei Key Laboratory of Emergency Rescue Technology, China People's Police University, Langfang, 065000, Hebei, China
[b] Hebei Key Laboratory of Hazardous Chemicals Safety and Control Technology, School of Chemical and Environmental Engineering, North China Institute of Science and Technology, Langfang, 065201, Hebei, China
[c] Guangzhou Liurui Firefighting Technology Co.,Ltd., Guangzhou, 510080, Guangdong, China
[d] National Engineering Laboratory for Fire and Emergency Rescue, China People's Police University, Langfang, 065000, Hebei, China

ARTICLE INFO

Keywords:
Thermal responsiveness
Microcapsules
Fluorinated liquids
Automatic fire-extinguishing
Fire safety performance

ABSTRACT

Most early-stage fires originating in small confined spaces may not be effectively mitigated by automatic fire-extinguishing systems. Leveraging the unique controlled release capability and barrier properties of microcapsules presents a promising avenue for developing multifunctional and intelligent fire-extinguishing agents tailored for early-stage fire suppression. This paper introduces two types of microcapsules that integrate automatic detection and fire extinguishing functions, utilizing fluorinated liquids specifically perfluoro(2-methyl-3-pentanone) and 1,1,1,2,2,3,4,5,5,5 decafluoro-3-methoxy-4(trifluoromethyl)-pentane as core materials. The preparation process was optimized, and the thermal response of the microcapsules was evaluated by directly incorporating them into combustible materials. The results indicated a correlation between the preparation method, coating efficiency, and thermal stability of microcapsules with the core-wall materials. When the fluoride solution in the core material reaches the thermal response threshold temperature, the gas pressure generated during vaporization and phase change can break through the shell, enabling early active fire protection. Beyond a specific threshold of additive microcapsules in the material, the material exhibits self-extinguishing potential during combustion. In cases where the additive amount falls short of achieving self-extinguishing, the fire-resistant performance of materials can be enhanced through various measures. For instance, reducing the amount of fire-extinguishing agents, delaying the ignition time of fuel, and lowering the heat release rate during combustion are effective strategies. Moreover, the degree of improvement is related to the additional amount and the type of core-wall materials. The thermal-response mechanism of microcapsules constitutes a comprehensive mechanism with physical and chemical effects. The finding of this research offer a new technical approach for microencapsulating high-boiling-point gas extinguishing agents, facilitating intelligent and precise prevention of early fires resulting from combustible materials.

* Corresponding author.
E-mail address: zhangman_hcsct@163.com (M. Zhang).

https://doi.org/10.1016/j.heliyon.2024.e27454
Received 19 December 2023; Received in revised form 25 January 2024; Accepted 28 February 2024
Available online 3 March 2024

List of symbols

PMP	Perfluoro (2-methyl-3-pentanone)
DMTP	1, 1, 1, 2, 2, 3, 4, 5, 5, 5-decafluoro-3-methoxy-4-(trifluorometyl)-pentane
UF	Prepolymer of formaldehyde solution and urea
SMA520	Styrene maleic anhydride co-polymer
rpm	revolutions per minute
PMMA	poly (methyl methacrylate)
DCM	dichloromethane
CTAB	cetyltrimethylammonium bromide
HFC-125	Pentafluoroethane
HFC-227ea	Heptafluoropropane
FPA	Fire propagation apparatus
FESEM	Field-emission scanning electron microscopy
ATR-FTIR	Fourier transform attenuated total reflection infrared spectroscopy
TG	Thermogravimetry
M_1	Mass of initial microcapsules(g)
M_2	Mass of destroyed microcapsules(g)
M_0	Total amount of core material(g)
SET	Self-extinguishing time(s)
MEC	Minimum extinguishing concentration(%)
$\dot{m}$	Gas mass flow(g min^{-1})
HRR	Heat release rate(kW)
pHRR	Peak heat release rate(kW)
mHRR	Mean heat release rate(kW)
t_{vap}	Vaporization time(s)
t_{mix}	Mixing time(s)
t_{induce}	Induction time(s)
TTI	Time to ignite

1. Introduction

Fire is one of the most prevalent disasters, posing a significant threat to public safety and social progress [1,2]. Over the period from 1997 to 2017, China witnessed a staggering 4.677 million fires, resulting in 41,391 fatalities, 46,605 injuries, and direct property losses totaling 46,776.4 million yuan [3]. A critical factor contributing to the substantial losses and casualties in fire incidents is the origin of over 90% of fires in small, confined spaces during their early stages. However, existing automatic fire-extinguishing systems primarily address larger spaces, with protective volumes ranging from tens to thousands of cubic meters. This mismatch makes it challenging to precisely locate small fire sources and automatically extinguish fires in these intricate spaces [4].

Given the characteristics of early-stage-limited burning areas, slow smoke flow, monimal radiant heat, and gradual spread controlling and extinguishing fires at this initial stage can significantly reduce costs and optimize the efficacy of fire suppression efforts. Early fires present challenges such as delayed detection and susceptibility to rapid spread. Several studies in the field of fire engineering have explored the application of safe and intelligent devices or technologies to implement accurate prevention and control measures for early-stage fires [5]. The literature often emphasizes the importance or detection of early-stage fires. For example, Wang et al. [6] explored the pyrolysis characteristics of bus ceiling materials to elucidate early-stage fire behavior, while Mahbub et al. [7] developed an embedded system with deployable software for intelligent lighting and ventilation, enabling real-time monitoring via smartphones or PCs through the HTTP protocol. Zeng et al. [8] established a numerical model validated by Alpert's original ceiling temperature and velocity data of large fire powers. Vasiliev et al. [9] investigated the synthesis of metal oxide materials with reduced sensitivity to water vapors. Additionally, Li et al. [10] provided a comprehensive review of recent advances on early-stage fire warning systems, covering mechanisms, performance, and perspectives. Thus far, a fully developed fire-extinguishing material or device has not been reported, with essential technologies are still at the proof-of-concept stage.

The unique response mechanism of microcapsules to thermal stimulation, triggering the release of core materials through temperature changes, endows these microcapsules with exceptional properties absent in many conventional core-shell structural materials. Consequently, this material has garnered significant attention from scholars, offering a new avenue for developing materials with specialized thermal-response properties [11–13]. For instance, flame-retardant microcapsules can be incorporated into lithium-ion battery electrolytes or diaphragms. During the initial stage of thermal runaway, the wall material releases the core material flame retardant in response to melting, enhancing battery safety without compromising capacity retention rates [14,15]. Given the ability of thermal-response microcapsules to perceive and adapt to environmental changes without manual intervention, a fire-extinguishing material based on these microcapsules could achieve precise and intelligent early-stage fire prevention in small restricted spaces.

The research and development of fire-related materials utilizing thermal-responsive microcapsules have predominantly centered

on flame-retardant materials rather than extinguishing materials. In instances where the ambient temperature of these materials, housing flame-retardant microcapsules, experiences abnormal increases (e.g., due to the thermal runaway of lithium-ion batteries or the initial ignition of combustible materials), the outer wall material of the microcapsules reaches its melting point. This release triggers core materials possessing flame-retardant properties, thereby preventing further fire occurrence. For instance, Chen et al. [16] employed microcapsule-modified lithium battery cathode material with inorganic flame retardants (ATH and AlOOH) and organic flame retardants (TPP) as the core material to forestall thermal runaway caused by cathodic chemical reaction. Baginska et al. [17] encapsulated flame-retardant TCP to diminish the flammability of lithium-ion battery electrolytes using a shell material with electrochemical stability. Simultaneously, Kazanci et al. [18] introduced halogen-free flame retardant into paraffin wax microencapsulation to mitigate the flammability of paraffin wax, among other applications. Comprehensive studies in the field of fire-extinguishing are limited.

From the perspective of fire-extinguishing microcapsules, fluorinated liquids, exemplified by perfluoro (2-methyl-3-pentanone) (PMP, $C_6F_{12}O$) and 1, 1, 1, 2, 2, 3, 4, 5, 5, 5-decafluoro-3-methoxy-4-(trifluoromethyl)-pentane (DMTP, $C_7H_3F_{13}O$), prove highly suitable as core materials. The consideration of PMP and DMTP as ideal halon substitutes has garnered attention from scholars in fire-extinguishing agent research due to their eco-friendly characteristics and effective fire-extinguishing performance [15,19–21]. Given their boiling points of 49.2 °C [22] and 88 °C [15], respectively, and the phase-change force generated by the volume expansion during the vaporization process, these fluorinated liquids exhibit the potential to rupture the microcapsule wall, making them ideal core materials. Indeed, several studies have reported on fire-extinguishing microcapsules employing fluorinated liquids as core materials. This can be attributed to the core materials quickly reaching the boiling point under fire conditions, vaporizing, and releasing the gaseous fire-extinguishing agent upon breaking the wall materials. For example, Vilesov et al. [23,24] prepared fire-extinguishing microcapsules with dibromomethane,1,1,2,2-tetrafluorodibromoethane(Freon 114B2), perfluorotriethylamine, 2-iodoheptafluoropropane(Freon 217I1), and PMP as core materials, respectively. The microcapsule walls were modified in both a double-layer and MMT-addition gelatin fashion to mitigate core material loss. A recent study by Lee et al. [25] further confirmed that double-layered polymer microcapsules containing fluorine-based non-flammable agents improve core material content and fire suppression performance compared with single-wall microcapsules. Zhang et al. [26] prepared fire-extinguishing microcapsules with MUF as the wall material and a core material comprising a PMP and heptafluorocyclopentane mixture to prevent fires triggered by lithium-ion batteries.

Few studies have focused on the properties of microcapsules related to fire extinguishing. Existing studies, limited in number, predominantly concentrate on core material the resistance and extinguishing efficiency, employing criteria that appear excessively restrictive in assessing advantages and disadvantages. A thorough evaluation of the reliability and efficacy of emerging technologies or materials in fire engineering is crucial, particularly in the absence of national standards [27]. Thermal stability, encompassing both fuel-related aspects [28] and hazardous chemicals like benzoyl peroxides containing metal ions [29], trinitrophloroglucinol [30], toluene sulfonation [31], nitrocellulose [32], firework propellants [33], and acetic anhydride [34], has been implicated in the development of thermal-response materials. Given its potential as a thermal-response material, the thermal stability of fire-extinguishing microcapsules of paramount importance. Furthermore, owing to the core-shell structure of composite materials, optimizing the preparation process for microencapsulation efficiency holds practical significance. Above all, assessing the thermal responsiveness under the direct action of flames or the indirect influence of flame radiation is imperative for positioning this microcapsule as a fire extinguishant.

This paper, therefore, employs the typical fluoride extinguishing agents PMP and DMTP as core materials to fabricate thermal-response fire-extinguishing microcapsules, examining the microencapsulation method, process optimization, and thermal behavior. Through the addition of microcapsules to materials, the paper evaluates the self-sustaining effect of thermal-responsive microcapsules in the initial stages of fires ignited by combustible materials using a standard Cup-burner and fire propagation apparatus (FPA). A series of experiments is conducted primarily to acquire additional parameters, aiding in model construction and enhancing accuracy for future work on simulating fire-extinguishing mechanism. The research outcomes present a novel technical approach for the microencapsulation of high-boiling-point gaseous fire-extinguishing agents and the precise prevention of early-stage fires ignited by combustible materials.

2. Experimental methods

2.1. Microcapsules preparation

2.1.1. UF@PMP microcapsules

In this study, UF@PMP microcapsules were prepared using in-situ polymerization, utilizing commercial chemicals without further purification. PMP served as the core material, while a prepolymer (UF), derived from the *in-situ* polymerization of formaldehyde solution (37% *wt*% in H_2O, Aladdin, China) and urea [$CO(NH_2)_2$] (AR, Aladdin, China), functioned as the wall material. Styrene maleic anhydride co-polymer (SMA 520) and *n*-octanol (AR, Aladdin, China) were employed as the emulsifying and antifoam agent, respectively. Additionally, formate (AR, Aladdin, China) and sodium hydroxide (NaOH) (AR, Aladdin, China) were used to initiate and catalyze polymerization by adjusting the solution pH. Deionized water (< 0.06 μS/cm) was employed in solution preparation.

First, 0.52g NaOH, 1g SMA520 and 50g deionized water were combined in a beaker and stirred to ensure complete solubility of SMA520. Simultaneously, another beaker was used to measure 27.5g of 37.5 *wt*% formaldehyde solution and adjust the pH to 8 with a 5 *wt*% NaOH solution. Then, 10.5g of $CO(NH_2)_2$ was weighed and added to the formaldehyde solution, stirring until complete dissolution. The beakers containing these two solutions were placed in a constant-temperature water bath. Once the temperature

reached 70 °C, the solutions were allowed to react for 1 h, followed by cooling to room temperature to obtain SMA520 solution and UF prepolymer solution.

After adding 50 mL of deionized water to a three-necked flask, mechanical stirring was initiated and maintained at a specific speed. Subsequently, a defined volume of the prepared SMA520 solution (water phase), UF prepolymer solution and PMP (oil phase) were separately introduced into the three-necked flask. The container was immersed in a constant-temperature water bath to achieve high-speed emulsification and dispersion of PMP. Upon adjusting the water bath temperature to 30 °C, formate was applied to set the pH to 2.5. As the temperature reached 35 °C, 25 mL of deionized water was added. This addition was repeated every 15min, for 1h, maintaining the temperature for 4h to obtain UF@PMP microcapsule suspension. Subsequently, the suspension underwent filtration, cleaning with deionized water at least three times, and natural drying at room temperature to yield UF@PMP microcapsules. The schematic preparation procedures of UF@PMP microcapsules are illustrated in Fig. 1(a).

2.1.2. PMMA@DMTP microcapsules

Solvent evaporation was employed in the preparation of PMMA@DMTP microcapsules. For microencapsulation, 1, 1, 1, 2, 2, 3, 4, 5, 5 - decafluoro-3-methoxy-4 (trifluoromethyl) - pentane (DMTP) served as the core material, and poly (methyl methacrylate) (PMMA) (heat-tolerant, Macklin, China) as the wall material. Dichloromethane (DCM) (AR, Macklin, China) and cetyltrimethylammonium bromide (CTAB) (concentration 99%, Macklin, China) were uti; ized as the organic solvent and surfactant, respectively. Deionized water (< 0.06 μS/cm) was employed in solution preparation.

PMMA was introduced into a beaker containing DCM, followed by thorough dissolution. Afterward, a specific quantity of DMTP was added to the beaker, and the components were mixed to create the organic phase solution. Another beaker was filled with deionized water, and a specific quantity of CTAB was weighed and added to prepare a 4 *wt*% CTAB aqueous solution.

The beaker containing the 4 *wt*% CTAB solution was placed in a thermostatic water bath, initiating mechanical stirring at a

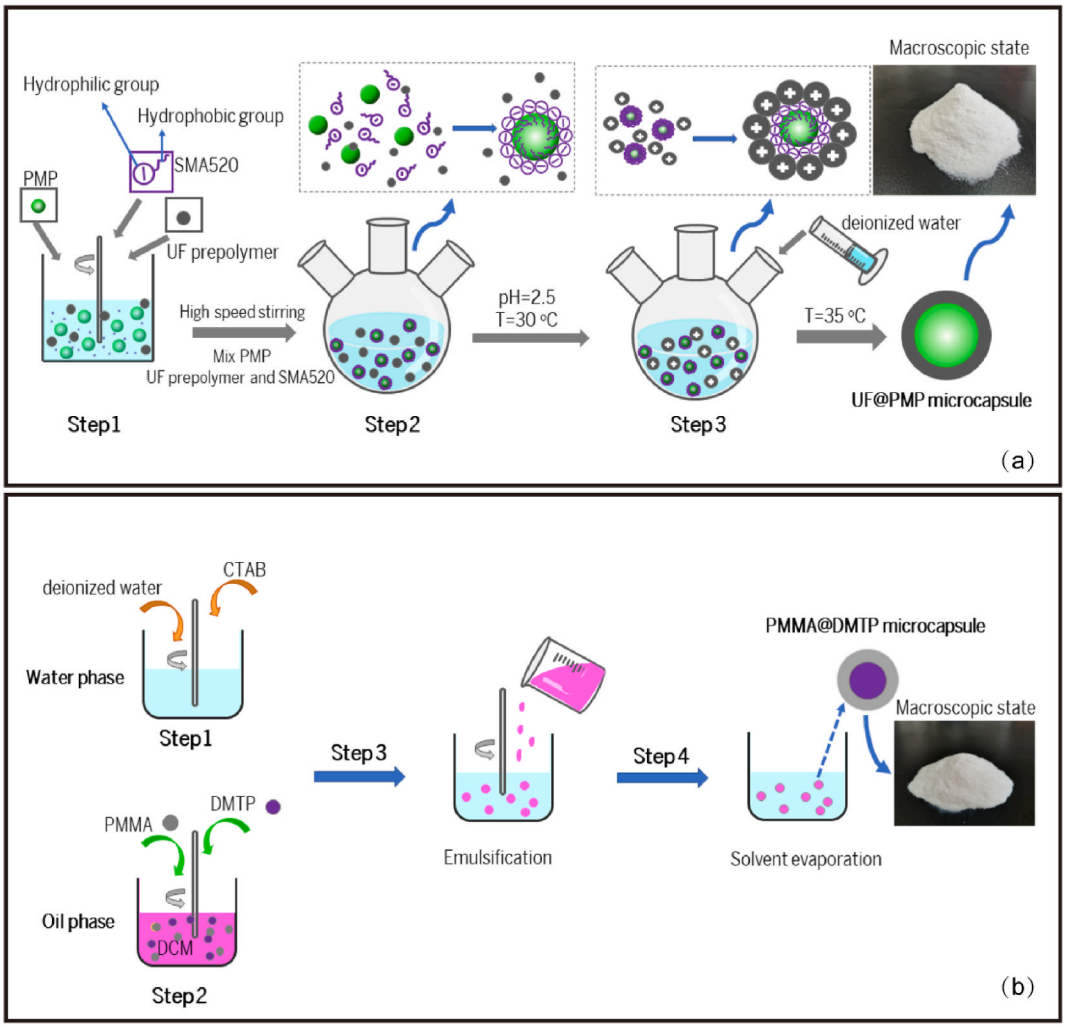

Fig. 1. Schematic of the preparation procedure for microcapsules. (a) UF@PMP; (B) PMMA@DMTP.

consistent speed. Concurrently, a pipette was used to slowly add the organic solution drop by drop into the solution over approximately 60 s. After adjusting the water bath temperature, the mixing speed remained constant for 3h to obtain the PMMA@DMTP microcapsule suspension. Subsequently, the suspension underwent filtration, and any residue on the surface was cleaned with deionized water. Finally, the experimental product was dried at room temperature to yield PMMA@DMTP microcapsules. The schematic preparation procedures for PMMA@DMTP microcapsules are depicted in Fig. 1(b).

2.2. Properties characterization

The micromorphology of microcapsules and its variations with changes in temperature were examined through field-emission scanning electron microscopy (FESEM) and a hot-stage polarization microscope [35]. The hot-stage microscope, equipped with a PixLink microscope camera (Canada PixLink Company), BHS polarized microscope (Japan Olympus Company), and THMESE600 heating stage (America Linkam Company), allowed for the observation of microcapsule suspension morphology. The average particle size was determined and recorded through Image PRO. Specifically, five arbitrary visual fields were selected from the surface of the suspension containing microcapsules for each sample. Image PRO software facilitated particle marking and size measurement, with about 50 microcapsules analyzed in each field. The particle size was calculated as the average of these 50 measurements. If the differences between the means of the five fields were less than 2 μm, the microcapsule dispersion level was considered satisfactory, and the final particle size was determined by averaging values obtained from the five fields.

The thermal characteristics of the microcapsules were investigated using the heating stage. A quartz crucible containing 2 g of the sample was placed on the heating stage, and the microscope was adjusted accordingly. A 20 × 10 magnification, focusing on observing multiple microcapsule particles, was adopted. The heating stage parameters were set at 20–300 °C with a heating rate of 10 °C/min. Linksys controlled the exposure time, and a microscopic imaging camera captured micrographs of microcapsule morphology as a function of temperature. Multiple parallel experiments were conducted to accurately determine the starting time of the phase transition.

For Fourier transform attenuated total reflection infrared spectroscopy (ATR-FTIR) analysis, which detects chemical functional groups in solids, gases, and liquids [36,37], Brooke TENSOR II conducted tests based on the microcapsule's structural strength. Background collection preceded spectrum capture for each sample, and then 3 mg of the sample was placed flat on crystal faces. For liquid-phase sample FTIR testing, an appropriate amount of liquid sample was directly introduced into the liquid pool, and the wavelength for the entire FTIR test range was 4000-500 cm^{-1}.

Thermogravimetry (TG), a widely used method for thermal stability and behavior testing, was employed to analyze the relationship between sample mass loss and temperature variation in different reaction stages [38–40]. NETZSCH Company's NETZSCITG 209 thermogravimetric analyzer was used for TG analysis in nitrogen purging gas, with an inlet speed of 50 mL/min, a heating temperature range of 25–800 °C, and a heating rate of 20 °C/min. Sample masses were maintained at 2.0 ± 0.1 mg, ensuring consistent relative filling amounts and particle sizes in the crucible before testing.

The encapsulation efficiency of the microcapsules was calculated using the following method. The naturally dried microcapsule sample with a mass of M_1 was ground to a powder with a mortar, and its capsule wall was destroyed. It was then washed with absolute ethanol and soaked for 24h to release the liquid-phase core material inside the microcapsule. Subsequently, the soaked sample was placed in a box with constant temperature and humidity. After heating at 130 °C for 12h, the sample was weighed and recorded as M_2. Finally, the encapsulation efficiency was calculated using Formula (1).

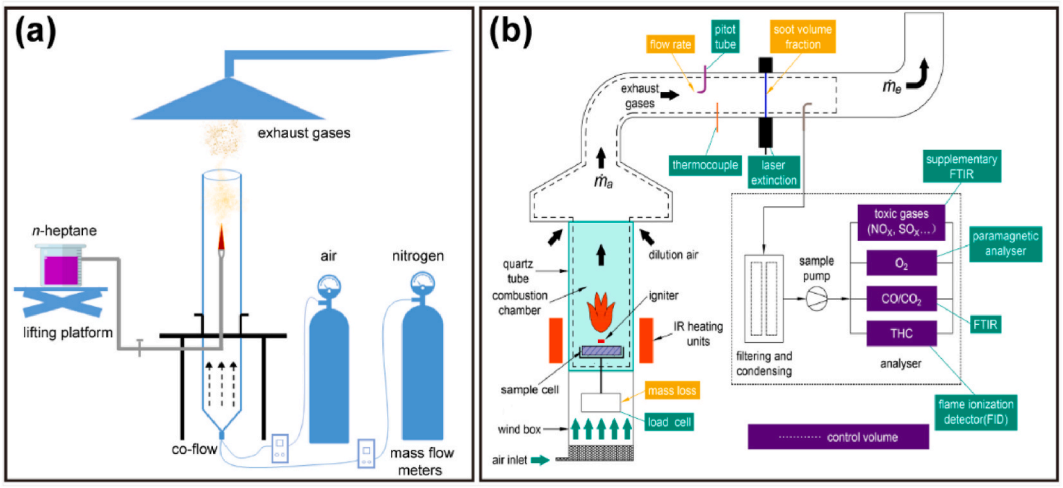

Fig. 2. Schematic of the experimental device. (a) Cup-burner; (b) FPA.

$$Encapsulated\ efficiency(\%) = \frac{M_1 - M_2}{M_0} \times 100 \quad (1)$$

M_0: Total amount of input core material during preparation (g).

2.3. Thermal-response efficiency

Considering the potential instability of the liquid core and the risk of agglomeration during the microcapsule drying process, thermal-response efficiency tests were conducted by directly adding the microcapsules to the fuel without undergoing drying. The mixture was stirred with a glass rod to ensure thorough homogenization of its contents. These experiments were conducted under conditions of 25 °C, 1.01 × 10^5 Pa.

A self-extinguishing experiment was employed to elucidate the impact of microcapsules on restricting fuel combustion [41–43]. Specifically, 2 mL of *n*-heptane was added to four surface dishes with a diameter of 5 cm. Subsequently, 0.2g each of UF@PMP, PMMA@DMTP, and ultrafine ABC powders were individually introduced into three of the surface dishes. The four surface dishes filled with *n*-heptane were then simultaneously ignited. The burning process of *n*-heptane was recorded using a camera, and the flame self-extinguishing time(SET) was measured with a stopwatch.

In cases where the quantity of added microcapsules was insufficient for self-extinguishment, the Cup-burner and FPA were employed to investigate the relationship between the percentage of microcapsules addition in the fuel and the self-extinguishing effect. The schematic diagram of the experimental device is presented in Fig. 2.

The Cup-burner test, a recognized laboratory-scale method for determining the fire-extinguishing concentrations of gaseous fire extinguishants, was utilized to assess the fire extinguishing efficiency by comparing the minimum extinguishing concentration (MEC) [44–46]. Given the stable flame provided by the Cup-burner, it was also employed to accurately evaluate the flame suppression effects of fire extinguishants. In this case, the agents were added to the fuel instead of the oxidizer, following a similar principle [47–49].

In this test, the combustion cup and the outer cover of the quartz tube were coaxial. The circular combustion cup, crafted from stainless steel, possessed an inner diameter of 25 mm and a thickness of 2 mm. A polished 45° chamfer adorned the edge of the cup mouth for smoothness. This combustion cup was seamlessly connected to an external tank containing liquid fuel. Simultaneously, the tank was positioned on a metal bracket with adjustable height to ensure that the fuel level in the combustion cup was consistently aligned with the cup mouth, maintaining flame stability. A three-layer 15.8 mesh/cm rectifier network positioned between the combustion cup root and the support base regulated airflow. The quartz tube had an outer diameter, thickness, and height of 90, 4, and 550 mm, respectively, with a maximum continuous-use temperature tolerance of 1050 °C. The coaxial setting included a diffusion chamber below the combustion cup with a height of 40 cm and two nested casings for oxidizer and fire-extinguishing agent supply. The mixture was homogeneously blended in the chamber, as depicted in Fig. 2 (a). The liquid fuel for the experiment was *n*-heptane, featuring microcapsules at varying additive mass fractions 0 *wt*%, 2 *wt*%, 4 *wt*%, 6 *wt*%, 8 *wt*%, and 10 *wt*%. Pre-dried compressed air (co-flow air) from an air compressor served as the oxidizer, stabilized at a flow rate of 40.0L/min (8.5 cm/s) through a mass flowmeter (Dmass, Flows Instruments Co., Ltd., accuracy ± 1.0%, repeatability is ±0.1%). This flow rate complied with data in the literature and satisfied ISO14520-1-2015 and NFPA2001-2018 flame height requirements. The flame was extinguished by introducing high-purity N_2 (99.99%) from a high-pressure gas cylinder to the co-flow air. Both gases were thoroughly mixed before entering the Cup-burner. The *n*-heptane in the burner burned for a minimum of 60 s before introducing N_2 to the co-flow air. Subsequently, the N_2 flow rate increased gradually, and the co-flow air rate decreased simultaneously, maintaining a constant total flow rate using the mass flowmeter. A minimum 10 s duration preceded the subsequent concentration adjustment of N_2 until flame extinguishment, and the MEC of N_2 was calculated using Equation (2).

$$\mathrm{MEC} = \frac{\dot{m}_{N_2}}{\dot{m}_{N_2} + \dot{m}_{air}} \times 100 \quad (2)$$

$\dot{m}$:Gas mass flow (g/min).

The FPA, following the standard ISO 12316 and ASTM E 2058, and illustrated in Fig. 2(b), was employed to investigate the combustion properties of combustible materials under varying radiant heat fluxes and oxygen concentrations. This apparatus comprises two main subsystems: the combustion control system and the combustion product test system [50,51].

In the combustion control system, 10 mL of *n*-heptane was introduced into five steel sample boxes measuring 0.1 m × 0.1 m with a thickness of 0.1 m. Subsequently, microcapsules with varying mass fractions 0 *wt*%, 4 *wt*%, 6 *wt*%, 8 *wt*%, and 10 *wt*%—were added to the n-heptane. Each mass fraction corresponded to a distinct FPA test. Placing the sample box on the sample table and covering it with quartz glass formed a combustion chamber for each set of mass fraction conditions. Outside the combustion chamber, four infrared heating devices were positioned, achieving convection through the lower air inlet. All combustion products, including combustion-supporting air, were drawn into the combustion product test system through the smoke exhaust pipe. The combustion product test system utilized a pitot pump, thermocouple, and laser device to measure the flow, temperature, and extinction coefficient of combustion products. A fraction of the fire smoke underwent dilution, filtration, and drying before component analysis in the gas analyzer during the sample combustion process, including O_2, CO, and CO_2 [52,53]. Following the calorimetric law of fire, the heat release rate (HRR) of *n*-heptane combusted with varying microcapsule additions could be calculated, taking the measured volume fraction of combustion product molecules as the input parameter. The *n*-heptane combustion experiment occurred under mixed gas with fixed oxygen concentration, supplied from a gas cylinder using a volume flow controller at a rate of 100L/min [54].The relatively low flow rate was set to preserve the buoyant and turbulent nature of the flames [51]. Considering the energy features of early-stage fire, the

external radiation heat flow intensity was set to 25 kW/m^2.

The sample error was assessed through occasional detection tests on the parameters measured by the self-extinguishing, Cup-burner, and FPA experimental system. Based on the original detection test results, the errors in the main results were estimated as the percentage of the absolute error and average value, i.e., relative error. The final errors of SET, MEC, and HRR were 2.7%, 10.2%, and 7.1%, respectively.

3. Results and discussion

3.1. Effects of preparation conditions on the properties of UF@PMP microcapsules

The influence of the volume of SMA520 solution (i.e., water-oil ratio) on sample preparation was investigated under conditions of UF prepolymer solution to PMP (oil phase) volume ratio 1.3:1 and mechanical stirring at 800 rpm. The results are depicted in Fig. 3.

The TG curve in Fig. 3 (a) illustrates the distinctive thermal weight-loss processes of the sample under various water-oil ratios. When the ratio was below 3:1, the sample experienced two prominent weight-loss processes. The initial temperature of the first loss, around 120 °C, signified the vaporization release of PMP. The second loss, beginning at approximately 250 °C, corresponded to the thermal decomposition temperature of UF [55,56]. As the water-oil ratio increased to 10:1, the sample displayed a singular, distinct loss process, nearly equivalent to the thermal decomposition of UF. The first loss correlated with the vaporization-phase transition of PMP, and the loss rate at this stage varied with the water-oil ratio. The loss rate of PMP initially decreased and then increased with the rise in the water-oil ratio, reaching a maximum of 58.3% at a water-oil ratio of 2:1, indicating the highest encapsulated PMP content. At a water-oil ratio of 10:1, the weight-loss rate was less than 10%, slightly differing from the empty shell. These results demonstrate that PMP microencapsulation was effective at water-oil ratios below 3:1. The microencapsulation efficiency of PMP decreased with increasing water-oil ratio beyond 3:1, eventually becoming impractical at 10:1.

The microencapsulation degree of PMP depends on the competition between emulsification on the core material and the electrostatic attraction on the wall material facilitated by SMA 520. Throughout the preparation process, PMP underwent emulsification and dispersion into oil droplets with a consistent particle size and specific surface area, guided by the action of SMA 520. SMA 520 serves as an amphoteric surfactant with a lipophilic end deposited onto the surface of PMP oil droplets. Simultaneously, the

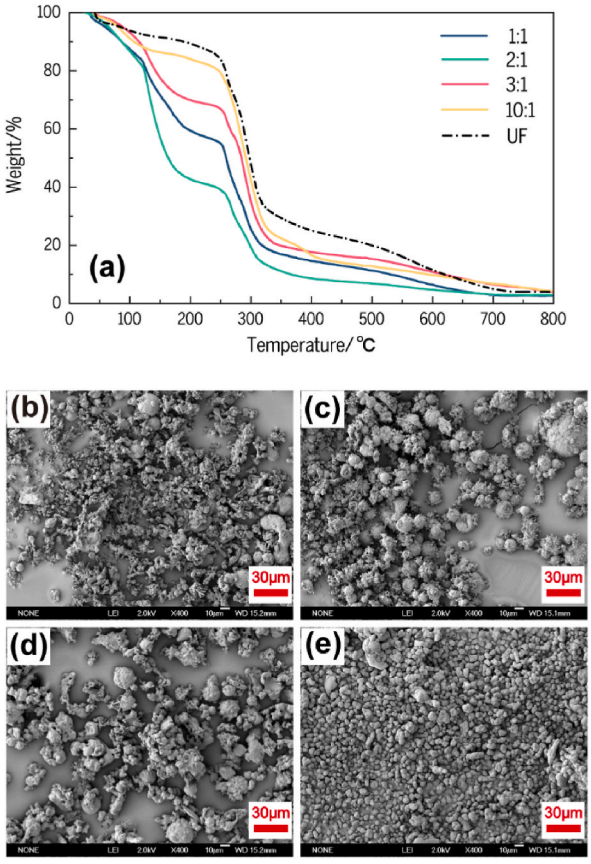

Fig. 3. Effects of water-oil ratios on PMP microencapsulation efficiency. (a) TG curves; (b)–(e) SEM images for UF@PMP microcapsules formed at different water-oil ratios: 1:1, 2:1, 3:1, and 10:1, respectively.

hydrophilic end exhibited an electrostatic attraction to the UF prepolymer, forming a fundamental core-shell structure [57]. At a water-oil ratio of 1:1, the insufficient quantity of SMA520 in the solution failed to emulsify and disperse all PMP oil droplets. The scarcity of SMA 520 on the oil droplet surface resulted in less UF, producing a thinner wall. Volatile PMP easily breached the wall material, generating a considerable amount of flaky material, as depicted in Fig. 3(b). With the gradual increase of SMA 520, more SMA520 on the oil drop surface and an augmented amount of attracted UF led to thicker microcapsule walls, reinforcing the core-shell structure. This process yielded numerous microcapsules with minimal cracks, characterized by regular and uniform morphology and particle size, as shown in Fig. 3 (c). As SMA 520 continued to increase, excessive deposition on the oil surface thickened the microcapsule walls, resulting in uneven particle size distribution (Fig. 3 (d)). Additionally, the surplus SMA 520, incapable of deposition on the core material surface, combined with the UF prepolymer through electrostatic attraction, forming UF microspheres instead of microcapsules (Fig. 3 (e)).

The impact of the core-wall ratio on sample preparation at a water-oil ratio of 2:1 and a mechanical stirring speed of 800 rpm was investigated. The research findings are presented in Fig. 4.

The TG curve depicted in Fig. 4 (a) illustrates that samples subjected to different core-wall ratios underwent two distinct loss processes. The initial weight-loss temperatures at 150 °C and 250 °C correspond to the vaporization release of PMP and the thermal decomposition of UF, respectively. Nevertheless, the core-wall ratio influences the sample's loss rate. Under a core-wall ratio of 1.3:1, the weight-loss rate reaches its peak, standing 1.33 times and 1.93 times higher than the ratios of 1:1 and 1.5:1, respectively. These findings underscore the correlation between the microencapsulation effect of PMP and the core-wall ratio.

The microencapsulation effect of PMP, when the core material content is fixed, is determined by the wall material. A surplus of wall materials adheres to the core material surface, forming UF@PMP microcapsules. Excessive wall materials undergo auto-polymerization, driven by the electrostatic attraction of SMA520, forming wall-material microspheres devoid of core materials [58], as illustrated in Fig. 4 (b). The coexistence of microcapsules and wall-material microspheres in the product results in notable particle size disparities and severe adhesion. When the quantity of wall material precisely meets the requirement to adhere to the core material's surface, most microcapsules take on a regular shape with uniform particle size, as depicted in Fig. 4 (c). With further reduction in the amount of wall material, insufficient wall material deposits on the core material surface, causing the microcapsule wall to thin and the binding force to weaken. This weakening results in core material leakage and the formation of numerous wall fragments, as shown in Fig. 4 (d).

The influence of stirring speed on sample preparation at a water-oil ratio and core-wall ratio of 2:1 and 1.3:1, respectively, was studied. The results are presented in Fig. 5.

According to the TG curve presented in Fig. 5 (a), samples subjected to different stirring speeds undergo two distinct transparent weight-loss processes with varying loss rates. Thus, UF@PMP microcapsules were prepared within a stirring speed range of 400–1200 rpm. Conversely, the weight-loss rate of the microcapsules increases by 55.8% when the stirring speed decreases to 400 rpm under a water-oil and core-wall ratio of 2:1 and 1.3:1 during the preparation process. This increase is1.4 times the weight-loss rate of microcapsules prepared at 1200 rpm. This phenomenon indicates that an appropriate stirring speed can enhance the core material

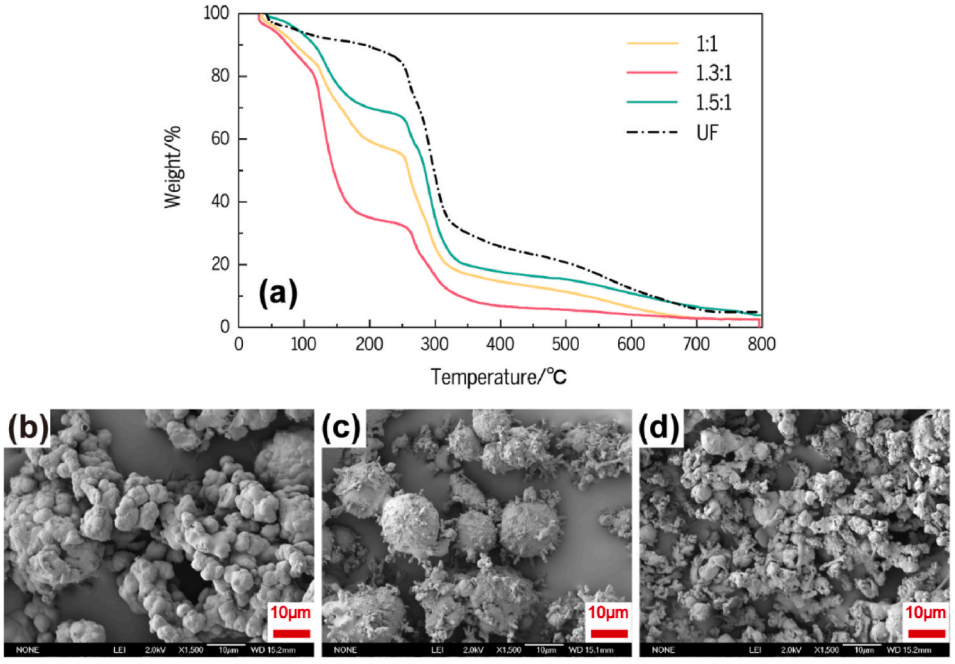

Fig. 4. Effects of core-wall ratios on PMP microencapsulation efficiency. (a) TG curves; (b)–(d) SEM images for UF@PMP microcapsules formed at different core-wall ratios: 1:1, 1.3:1, and 1.5:1 respectively.

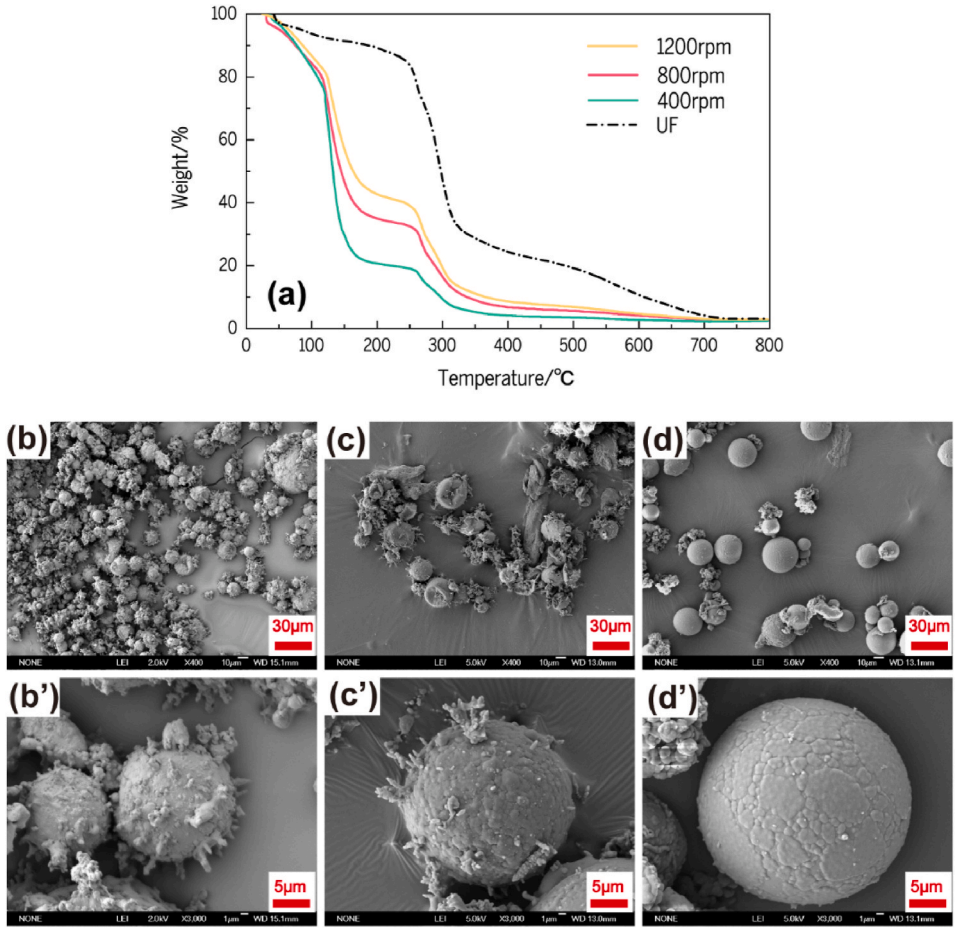

Fig. 5. Effects of stirring speed on PMP microencapsulation efficacy. (a) TG curves; (b)(b')-(d)(d') SEM images for UF@PMP microcapsules formed at different stirring speed: 1200, 800, and 400 rpm, respectively.

content. At high stirring speeds, numerous UF oligomers adhere to the inner wall of the three-necked flask due to the adhesiveness of UF [59]. In this process, the solidification results in the formation of many white precipitates, as depicted in Fig. 5 (b), leading to a reduction in the quantity of wall material. The decrease in wall material on the surface of the core material leads to a higher concentration of SMA520 branches remaining on the microcapsules' surface, as shown in Fig. 5 (b'). Further reduction in stirring speed

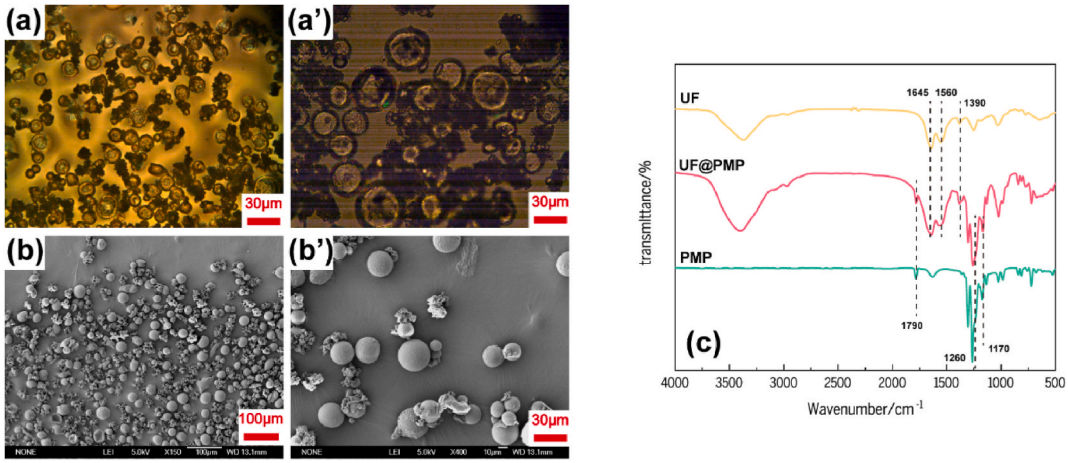

Fig. 6. Microscopic morphology of UF@PMP microcapsules. (a)(a') microcapsules in turbid liquid; (b)(b') microcapsules after drying; (c) FTIR.

results in decreased adhered UF, white precipitates participating in the reaction, and SMA520 branches, as shown in Fig. 5 (c) (c') (d). At a stirring speed of 400 rpm, the microcapsules exhibit a dense and smooth structure with uniform size. Although the experiment's stirring speed range is broad, the weight-loss rate of the microcapsules remains above 50%, indicating that the influence of stirring speed on PMP microencapsulation is weaker compared with the water-oil and core-wall ratios.

In conclusion, the key factors influencing PMP microencapsulation in this study are the water-oil ratio, core-wall ratio, and stirring speed. The optimal preparation parameters corresponding to these factors are 2:1, 1.3:1, and 400 rpm. The micromorphology and the infrared absorption spectrum of UF@PMP microcapsules obtained under optimal preparation conditions before and after drying are shown in Fig. 6.

As illustrated in Fig. 6 (a) and (a'), the microcapsule sample prepared under optimized conditions exhibits regular spherical morphology with fine dispersibility and an average particle size in the solution. While a few UF particles without the cyst wall are present in the aqueous phase, there are minimal lumps, and no depressions were observed in the cyst wall. The spherical characteristics of the dried microcapsules are more apparent, with intact capsule walls and no cracks or gaps, as shown in Fig. 6 (b) (b'). Notably, the microcapsules maintained their structural integrity before and after drying, displaying no signs of collapse or wrinkling. This phenomenon underscores the efficacy of UF as the wall material in encapsulating PMP for microencapsulation.

As illustrated in Fig. 6(c), both the microcapsules (UF@PMP) and wall materials (UF) exhibit a stretching vibration absorption peak associated with $–NH_2$ and N–H in the range of 3500-3000 cm^{-1}. Additionally, a C–H stretching vibration absorption peak at 2971 cm^{-1}, a robust absorption peak of C═O stretching vibration in the amide bond at 1645 cm^{-1}, a prominent absorption peak of C–N

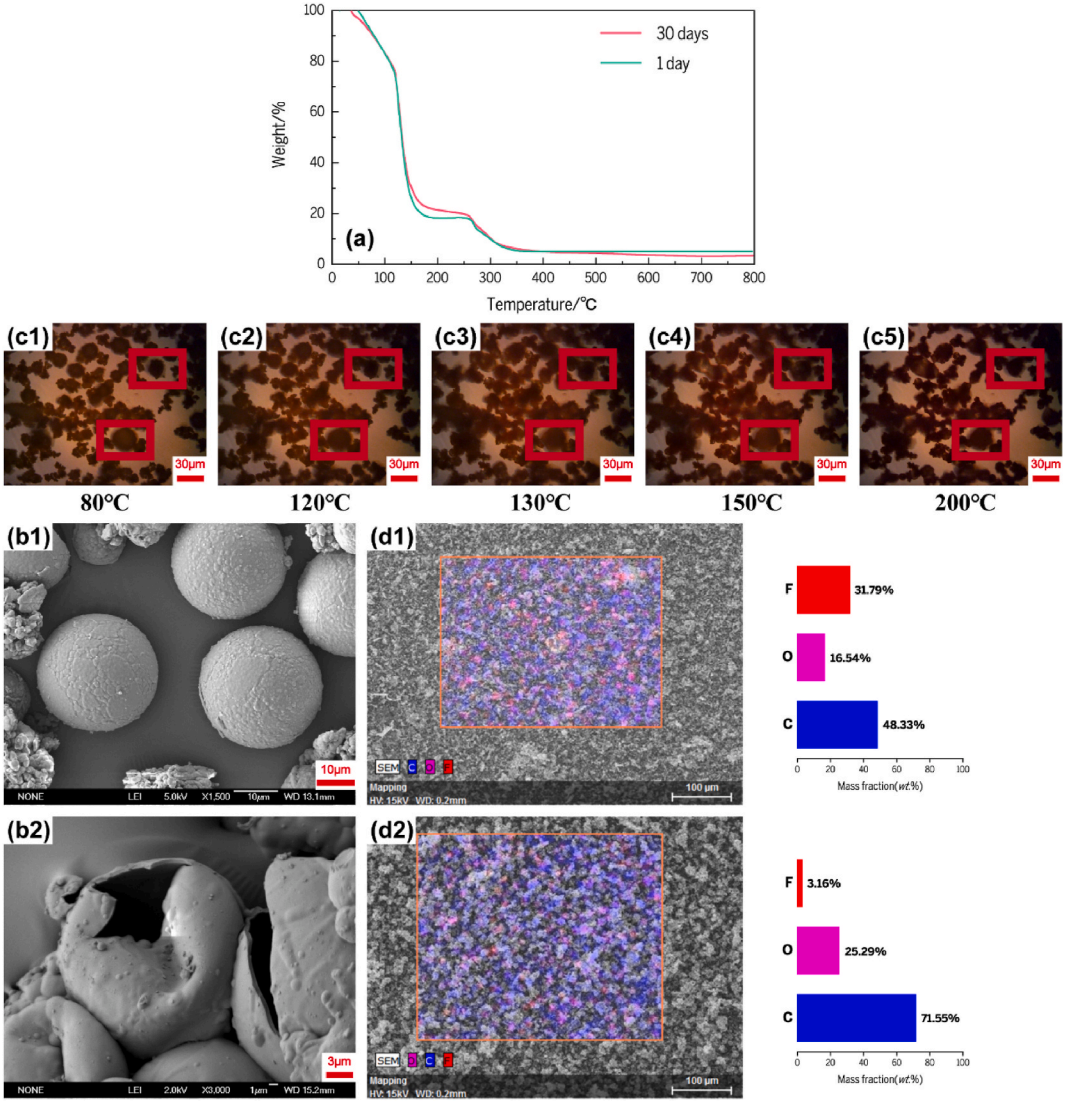

Fig. 7. Thermal stabilities of UF@PMP microcapsules. (a) storage stability; (b1)-(b2) microcapsules before and after core materials releasing; (c1)-(c5) variation of morphology with temperature; (d1)-(d2) surface element analysis before and after core materials releasing.

stretching vibration in the amide bond at 1560 cm^{-1}, and a C–H curling vibration absorption peak at 1390 cm^{-1} are observed [60]. None of these peaks are attributed to PMP, indicating that the microencapsulated shell of PMP comprises UF. Furthermore, the absorption peak of C═O stretching vibration in ketones appears at 1790 cm^{-1}, and the strong absorption peak of C–F stretching vibration in the range of 1350 cm^{-1} to 1100 cm^{-1} [61] is absent in the infrared spectrum of UF wall material. This evidence confirms the presence of PMP core material in the microcapsules. Notably, the C═O and C–F stretching vibration peaks also appear in the FTIR of microcapsules because the microcapsules prepared using in-situ polymerization in this study do not form fully enclosed core-shell structures but porous structures. Coupled with the high saturated vapor pressure of PMP, it slowly leaks during storage. Therefore, thermal stability is of interest.

The thermal stability of UF@PMP microcapsules obtained under optimal preparation conditions is depicted in Fig. 7.

As illustrated in Fig. 7 (a), the TG curves of UF@PMP microcapsules and microcapsules stored in an open space for 30 days exhibit a high degree of coincidence. This outcome indicates the excellent stability of UF for PMP microencapsulation through in-situ polymerization, promoting long-term storage. Simultaneously, the TG curve reveals that 120 °C marks the initial temperature for a significant increase in the microcapsule weight-loss rate, signifying the onset of wall material rupture. The first loss is completed at 150 °C, with the weight-loss rate exceeding 70%. The micromorphology of the microcapsule sample at 150 °C is depicted in Fig. 7 (b1) and (b2). The thick wall of a microcapsule ruptures under substantial internal stress, but the morphology of the remaining wall material remains visible at the thermal decomposition temperature of the wall material. This finding affirms that the phase-change force of the core material propels the rupture mechanism of UF@PMP. The observation result of UF@PMP by a hot-stage microscope is shown in Fig. 7 (c1) - (c5), indicating that the microcapsule volume increases initially and then decreases with increasing temperature because of the inherent elasticity of the UF wall material [62]. The phase-change force of the microcapsule in the thermal environment induces rupture in the wall material. When the temperature is low, the PMP core material vaporizes slowly, generating gas that increases the microcapsule volume while retaining the elastic modulus of the UF wall material, preventing microcapsule rupture. As the temperature increases, the core material vaporization rate accelerates, and the phase-change force surpasses the elastic modulus threshold of the UF wall material, enabling the release of gas. Once the volume decreases until the core material is released, the size stabilizes. Fig. 7(d1) and (d2) present EDS elemental analysis of Fig. 7 (b1) and (b2). It is observed that the content of F elemental in the microcapsule before core material release is notably higher than that after core material release. Specifically, the weight percent of the F element decreases from 31.79% to 3.16%, confirming that the PMP core materials are encapsulated within the microcapsule. The cracked microcapsule exhibits a relatively low F content compared with the intact one, confirming the release of the fire-extinguishing agent (PMP) after microcapsule rupture on the one hand and corroborating the porous structure of the microcapsules, as illustrated by the FTIR analysis of microcapsules. These results comprehensively demonstrate the successful preparation of UF@PMP microcapsules in this study.

3.2. *Effects of preparation conditions on the properties of PMMA@DMTP microcapsules*

The microencapsulation of DMTP in this study is influenced by core parameters, namely stirring speed, reaction temperature, and core-wall ratio. Table 1 illustrates the encapsulation efficiency and average particle size of PMMA@DMTP microcapsules, while Fig. 8 presents their microscopic morphology.

The encapsulation rate of microcapsules exhibits an initial increase followed by a decrease with rising stirring speed, reaction temperature, and core-wall ratio. This trend can be attributed to the dependency of microcapsule encapsulation on the curing rate of wall materials and the diffusion rate of core materials during solvent evaporation. Increased stirring speed and reaction temperature accelerate DCM evaporation, enhancing the PMMA wall material's curing rate and surpassing the diffusion rate of the core material into the aqueous phase, thus increasing encapsulation efficiency. However, higher stirring speeds concurrently reduce the particle size of microcapsules, causing breakage under intense shear forces and lowering encapsulation efficiency. Elevated reaction temperatures, approaching or exceeding the boiling point temperature of DCM (38.5 °C) [63], increase the curing rate of PMMA but also elevate the diffusion rate of DMTP. This imbalance leads to significant PMMA loss, resulting in decreased encapsulation efficiency.

As illustrated in Fig. 8 (a) - (a'') and Fig. 8 (b) - (b''), microcapsules observed under the optical microscope exhibited varying sizes

Table 1
Preparation conditions, encapsulated efficiency, and average particle size.

Preparation conditions		Encapsulated efficiency/%	Average particle size/μm
Stirring speed/rpm	800	22.3	58
	1000	25.5	49
	1200	47.2	35
	1600	29.2	19
Reaction temperature/°C	25	20.1	48
	30	49.8	66
	35	35.2	32
	40	9.7	10
Core-wall ratios	1:2	15.2	20
	1:1	23.8	40
	2:1	42.2	55
	3:1	12.5	72

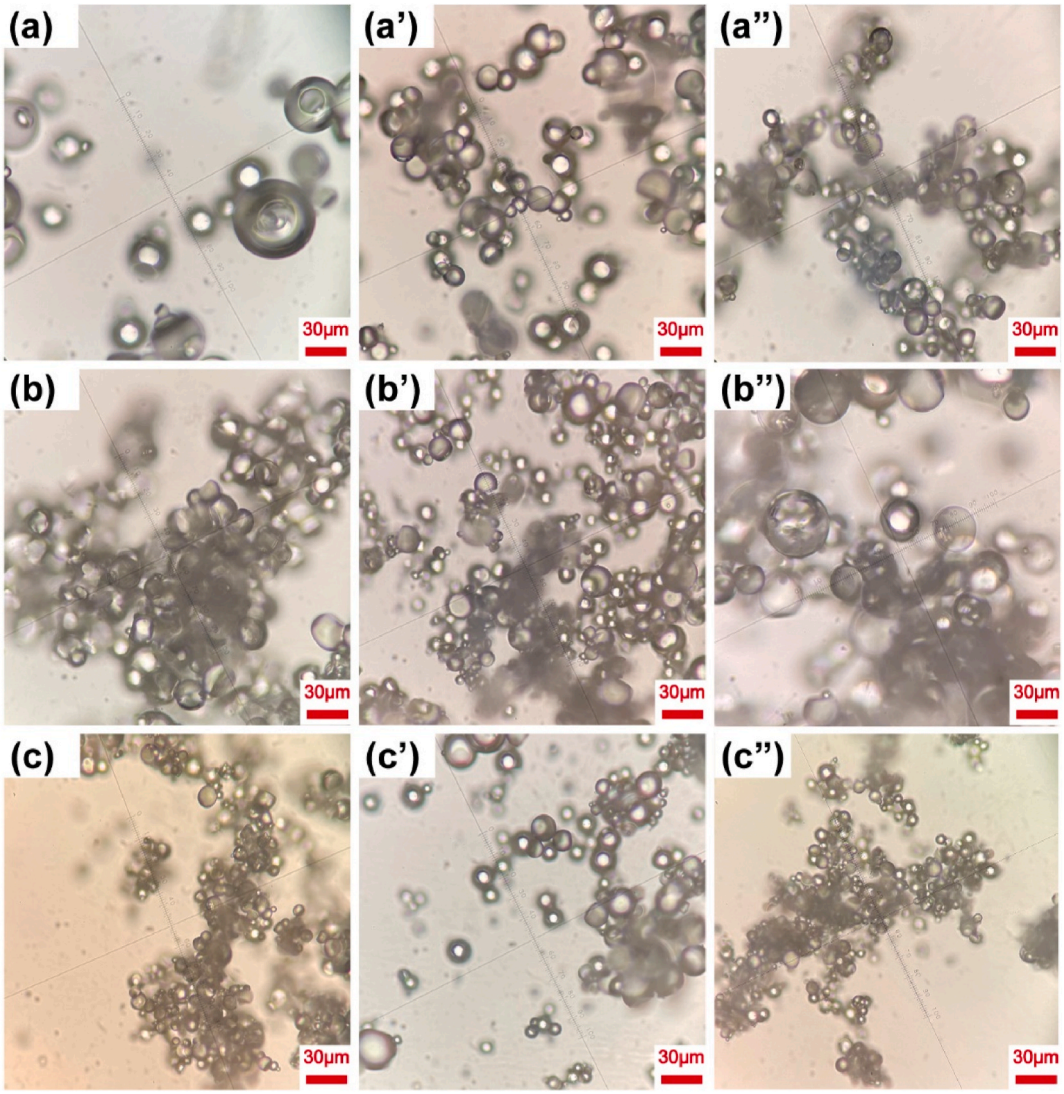

Fig. 8. Microscopic morphology of PMMA@DMTP microcapsules prepared in different conditions. (a)-(a'') stirring speeds are 800, 1200, and 1600 rpm respectively; (b)-(b'') reaction temperatures are 25, 30, and 35 °C respectively; (c)-(c'') core-wall ratios are 1:2 , 2:1, and 3:1 respectively.

when the stirring speed and reaction temperature were low. Additionally, agglomeration occurred, especially at 25 °C. Conversely, microcapsules prepared at 1200 rpm and 30 °C exhibited regular shapes, abundant quantities, and uniform particle sizes. Increased stirring speed to 1600 rpm resulted in numerous observable microcapsules. However, at a temperature of 35 °C, empty shells emerged due to core material diffusion. Notably, at 40 °C, empty shells could not form.

The influence of the core-wall ratio on the encapsulation rate of PMMA@DMTP is contingent upon the impact of oil viscosity on the curing rate of PMMA [64]. Oil viscosity decreased with diminishing PMMA concentration, leading to particle agglomeration, as depicted in Fig. 8 (c). Reduced oil viscosity, facilitated by an increased amount of core material, enhanced the curing rate of the wall material, promoting microcapsule formation, as illustrated in Fig. 8 (c'). Further augmentation of the core material, however, impeded its dispersion in the aqueous phase, resulting in larger particle sizes. Concurrently, insufficient PMMA hindered the encapsulation of larger core material droplets, forming thinner wall materials and making the microcapsules prone to breakage, as evident in Fig. 8 (c'').

In summary, the principal factors impacting PMMA@DMTP microencapsulation are stirring speed, reaction temperature and core-wall ratio. The optimal preparation parameters corresponding to enhanced encapsulation efficiency are 1200 rpm, 30 °C, and a core-wall ratio of 2:1. The chemical composition, thermal stability, and micromorphology of PMMA@DMTP microcapsules under these optimal conditions are illustrated in Fig. 9.

As illustrated in Fig. 9 (c) and (c'), the microcapsule sample prepared under optimized conditions, exhibits a regular spherical shape, with a uniform distribution of particle sizes, a smooth surface, a complete capsule wall, and no cracks or gaps. This observation underscores the applicability of PMMA as a suitable wall material for the encapsulation of DMTP, resulting in effective DMTP microencapsulation. The FTIR diagram of the PMMA@DMTP microcapsule is presented in Fig. 9 (a). The absorption peak at 1260 cm^{-1}

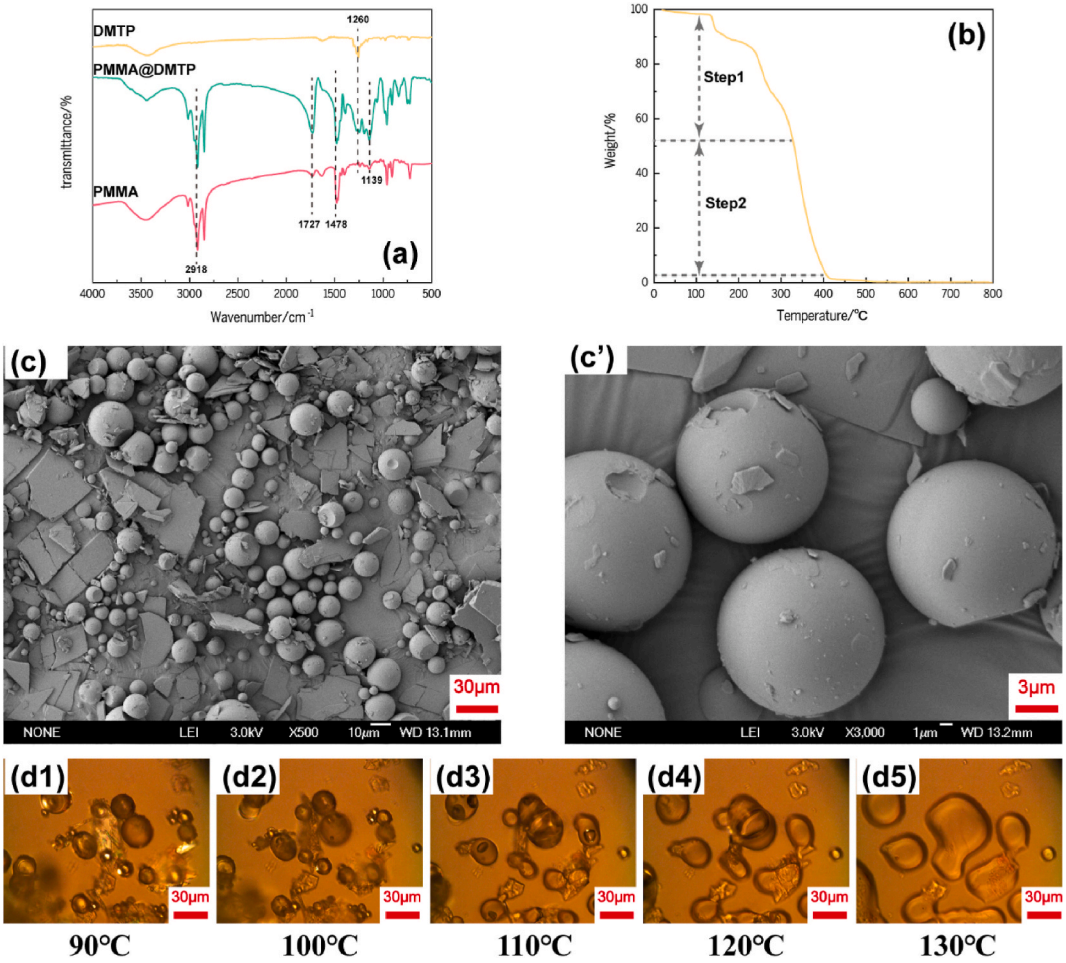

Fig. 9. Chemical composition, thermal stability and morphology of PMMA@DMTP microcapsules. (a) FTIR; (b) TG curves; (c)(c') SEM images; (d1)-(d5) variation of morphology with temperature.

corresponds to the asymmetric stretching vibration of the C–O–C bond in DMTP. Notably, the robust at 1727 cm^{-1} represents the C═O stretching vibration, while the unique stretching vibration absorption peak of PMMA is evident at 1139 cm^{-1} [65,66]. Furthermore, the bending vibration and stretching vibration absorption peaks of C–H in PMMA are identified at 1478 cm^{-1} and 2918 cm^{-1}. In the FTIR diagram of the PMMA@DMTP microcapsule, characteristic absorption peaks resembling PMMA emerge at 1139 cm^{-1}, 1478 cm^{-1}, 1727 cm^{-1}, and 2918 cm^{-1}. Additionally, a weak peak is detected at 1260 cm^{-1}. This phenomenon indicates the concurrent presence of PMMA and DMTP in the microcapsule. The appearance of the core material characteristic peak may be attributed to residual DMTP on the surface of the wall material. Consequently, researchers initially concluded that PMMA is effective in micro-encapsulating DMTP.

As illustrated in Fig. 9 (b), the sample undergoes two weight-loss processes, with initial temperatures of 95 °C and 320 °C, corresponding to DMTP release and the thermal decomposition of PMMA [67]. The boiling point of DMTP is 88 °C, and the glass transition temperature of PMMA is 122 °C [68]. Based on these findings, researchers infer that the rapid vaporization of the core material DMTP generates pressure, breaking through the wall material. In Fig. 9 (d1) - (d5), the microcapsule volume expands with increasing temperature. The microcapsule ruptures when the temperature is between 90 °C and 100 °C. Beyond 120 °C, the glass transition process of PMMA is observable. Simultaneously, PMMA droplets form at around 130 °C. However, the microencapsulation of DMTP does not significantly impact its phase-transition temperature. Moreover, the glass transition temperature of PMMA is close to the boiling point of pure DMTP, resulting in a significant decrease in the thermal insulation performance of the wall material during glass transition. The weight-loss rate in the first stage is 48.9%, indicating that the core fire-extinguishing components in PMMA@DMTP microcapsules constitute close to 50%. The lower data compared with UF@PMP microcapsule content(> 70%) is attributed to the preparation method and the selection of core and wall materials. The weight-loss rate in the two stages approaches 100% due to the vitrification of PMMA after heating. The appearance of PMMA is similar to liquid fuel with minimal evaporation residue [68], aligning with previous research results on the combustion characteristics of pure PMMA [69].

3.3. Effects of microcapsules on fire safety enhancement of combustible materials

The combustion process of the *n*-heptane with microcapsules is shown in Fig. 10.

The flame height of *n*-heptane decreases with time, entering the combustion attenuation stage around 40 s until it extinguishes at 60 s (Fig. 10 (a)). Compared with the absence of solid particles, the addition of ultrafine ABC powder does not alter the combustion state of *n*-heptane (Fig. 10 (b)). Notably, the flame height and brightness of *n*-heptane with microcapsules are significantly lower than those with ultrafine ABC powder. The flame of *n*-heptane with microcapsules enters the decay stage at 25 s and extinguishes at 36 s, as illustrated in Fig. 10 (c). Furthermore, *n*-heptane with UF@PMP microcapsules exhibits a more pronounced combustion inhibition effect. The flame height is halved within the first 5 s of microcapsule ignition, entering the decay stage at 10 s and extinguishing at 21 s, as depicted in Fig. 10 (d). PMMA@DMTP and UF@PMP microcapsules enhance the SET of *n*-heptane by 40% and 65%, respectively. This result signifies a substantial improvement in the SET of combustible substances facilitated by PMMA@DMTP and UF@PMP microcapsules. Notably, the UF@PMP microcapsules demonstrate a more pronounced effect.

The variations in the combustion of *n*-heptane with different microcapsule dosages are depicted in Fig. 11.

The combustion of pure *n*-heptane reveals a blue flame at the lower end and a yellow flame at the upper end. The flame exhibits a streamlined contraction because the fuel velocity and buoyancy-induced flow are slower than the co-flow air velocity [70]. In the vicinity of the buoyancy-induced flow guidance region, the flame pulsates due to instability, displaying a pulsating frequency of approximately 6 Hz. The brightness of the primary flame intensifies with an increasing concentration of microcapsules. The flame tip becomes thin and dark orange, while the blue base weakens and eventually disappears with increasing microcapsule concentration. The wall material of PMMA@DMTP microcapsules is composed of PMMA. Additionally, the core material, rich in hydrogen, releases more hydrocarbons during combustion. Consequently, the flame of *n*-heptane with PMMA@DMTP appears brighter compared with that with UF@PMP. The varying dosages and types of microcapsules correspond to distinct combustion states of *n*-heptane, signifying

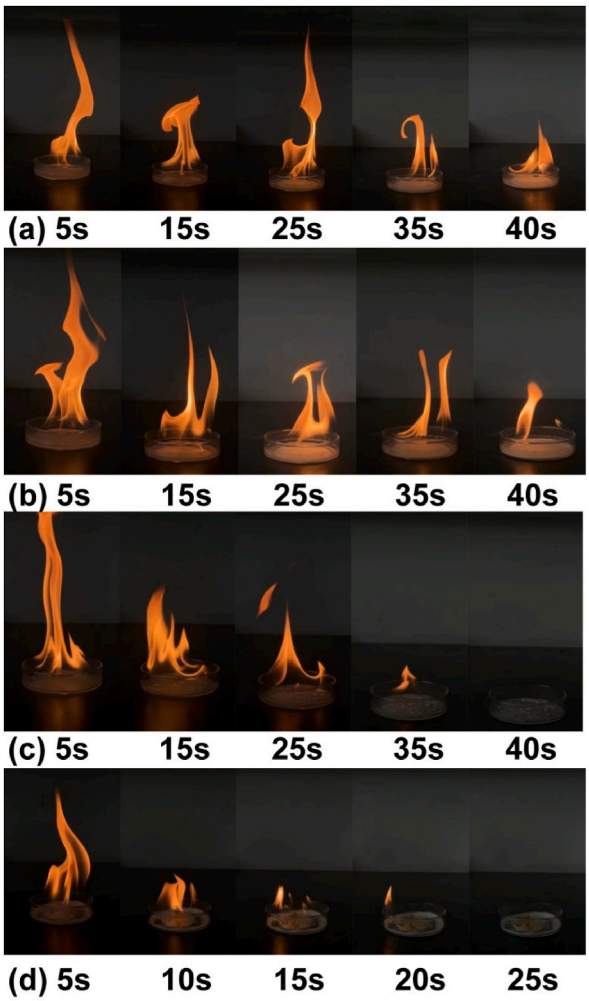

Fig. 10. Combustion process of *n*-heptane with and without additives. (a) without addition; (b) with Ultrafine ABC powder; (c) with PMMA@DMTP microcapsules; (d) with UF@PMP microcapsules.

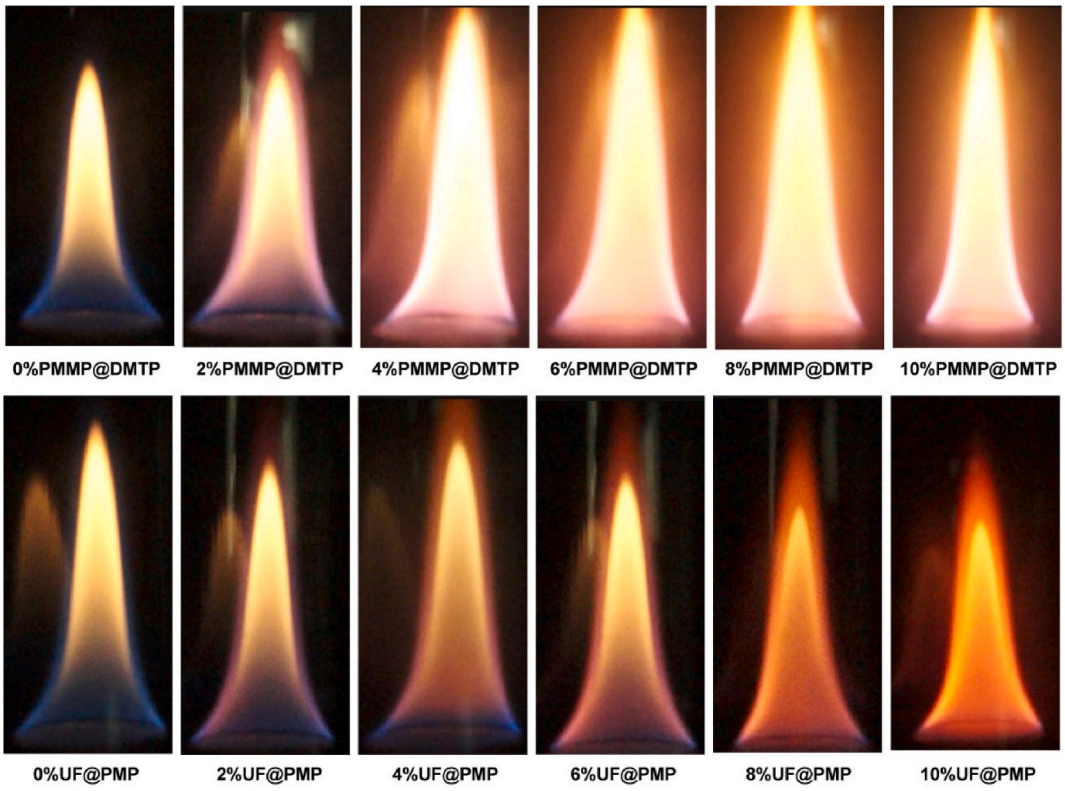

Fig. 11. Flames of *n*-heptane corresponding to different microcapsule dosages.

their influence on the fire-extinguishing process with different extinguishing agents.

Fig. 12 depicts the process and MEC of N_2 inhibiting and extinguishing the flame of the *n*-heptane with additive microcapsules.

Fig. 12 (a1) - (a6) and (b1) - (b6) illustrate the characteristic extinguishing process of the Cup-burner. Before the introduction of N_2 into the flame, it burned with a conical angle at the combustion cup mouth. As N_2 was introduced by the co-flow gas and diffused into the flame region, the boundary between the blue and light yellow in the flame disappeared. Throughout this process, the flame's brightness decreased, height increased, and flash frequency intensified, but the flame root remained stable. With a further increase in concentration, the flame's flicker frequency increased. Subsequently, the flame shape ceased to be conical, and the tip gradually vanished. The brightness of the flame root diminished, and it started moving away from the burner edge. When the N_2 concentration approached the MEC, the flame exhibited vigorous vibrations, and the root departed from the burner, seeking a new stable point. If the flame moved several millimeters away from the burner edge, it failed to return to the combustion cup mouth, resulting in extinguishment.

As illustrated in Fig. 12 (c) and (d), the MEC for suppressing and extinguishing the *n*-heptane flame with N_2 in this experiment is 33.1%, which is within 10% of the literature value, indicating high reliability of the gas flow field in the experimental setup. The MEC of N_2 decreased with increasing concentrations of PMMA@DMTP and UF@PMP microcapsules in *n*-heptane. The addition of 2% PMMA@DMTP and UF@PMP microcapsules reduced the MEC of N_2 by 24.2% and 26.3%, suggesting that incorporating microcapsules into the fuel could diminish the amount of fire-extinguishing agents needed. However, the effects varied with different microcapsules. Although the MEC of PMMA@DMTP microcapsules increased from 2% to 10%, the reduction in MEC was lower than the experimental uncertainty, implying that the increased mass fraction of PMMA@DMTP microcapsules did not significantly decrease the fire-extinguishing agent quantity. In contrast, the MEC of N_2 decreased with the increasing mass fraction of UF@PMP microcapsules in *n*-heptane. At an additive amount of 10%, MEC decreased by 53.5%, indicating that UF@PMP microcapsules had a more pronounced effect in reducing fire-extinguishing agents.

Fuel HRR denotes the rate of heat release per unit area after sample ignition, a crucial parameter for evaluating the thermal hazard of fuel in fires [75]. The HRR during the combustion of *n*-heptane with microcapsules is depicted in Fig. 13.

Typical *n*-heptane combustion unfolds in distinct stages, namely ignition, combustion, and extinguishing. During ignition, *n*-heptane absorbs external radiant heat and vaporizes, resulting in nearly zero HRR. The subsequent flaming combustion stage hinges on the evaporation rate, where the feedback heat from fuel combustion accelerates *n*-heptane vaporization, leading to a peak HRR (pHRR). The extinguishment stage, marked by insufficient fuel, manifests a sharp HRR decline.

The combustion of liquid fuel typically involves the combustion of vaporized steam [76]. The vaporization time (t_{vap}) denotes the period for n-heptane to transform into steam. Gaseous combustible mixtures form on the liquid surface through diffusion and

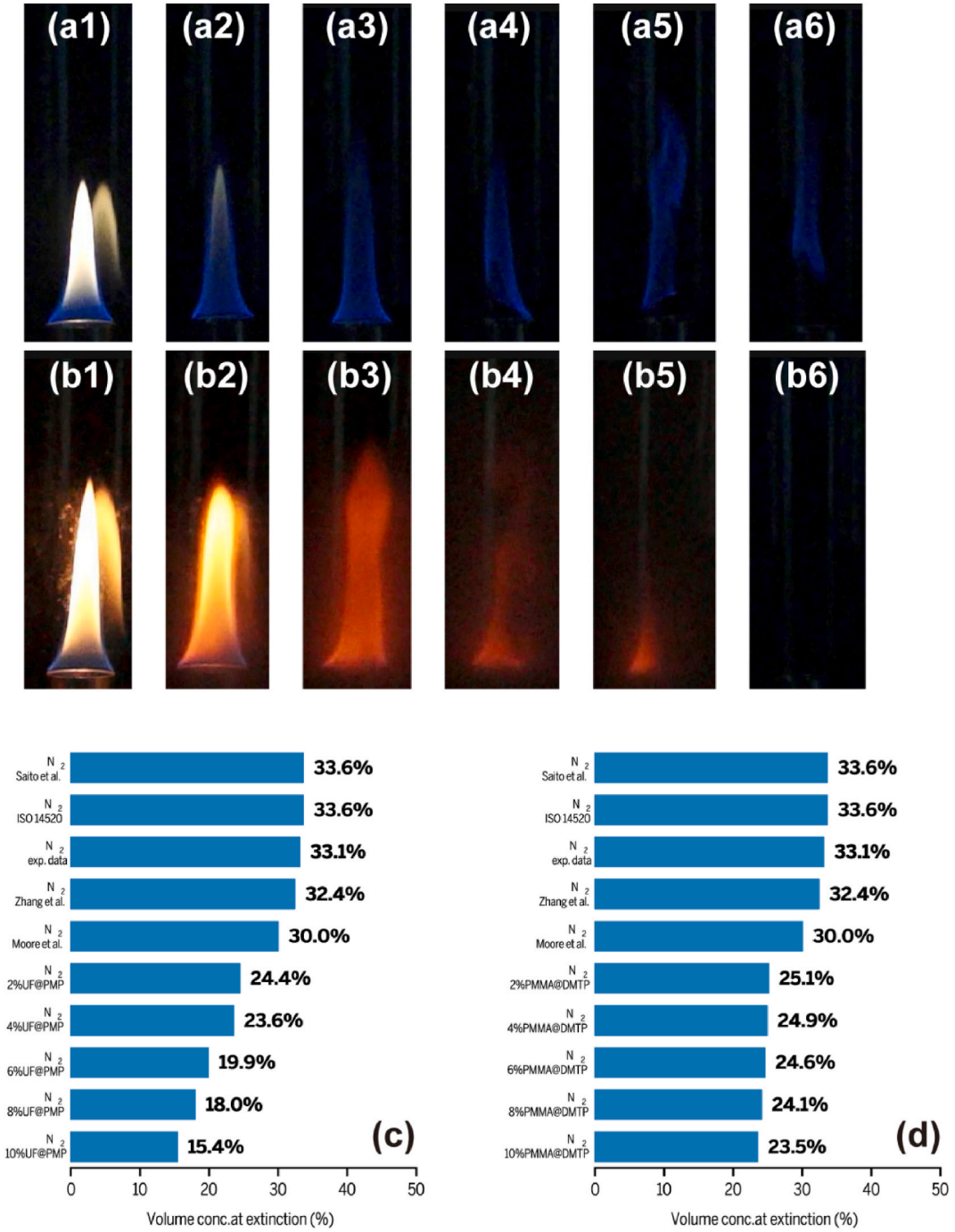

Fig. 12. MECs of microcapsules added to *n*-heptane/air Cup-burner flames with N_2. *exp.data* represents measured values, and *lic.data* denotes the values reported by Saito et al., ISO 14520, Zhang et al., and Moore et al. [71–74].

convection, mixing with the surrounding oxidant. As n-heptane vaporizes, the combustible mixture increases, reaching the lower combustion limit. The time from vaporization to the lower limit of combustion is the mixing time (t_{mix}). Upon reaching the ambient temperature threshold (corresponding to the induction time t_{induce}), the mixture ignites, giving rise to a flame. The ignition time (TTI), representing the duration from fuel exposure to a certain intensity of radiant heat until sustained ignition, is the sum of vaporization time, mixing time and induction time [77].

$$TTI = t_{vap} + t_{mix} + t_{induce} \tag{3}$$

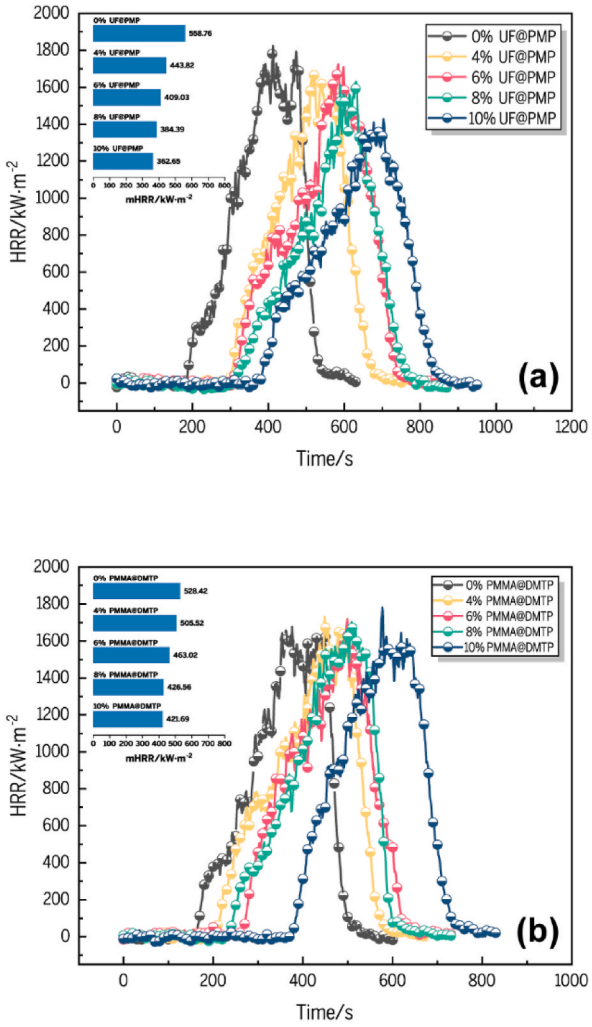

Fig. 13. Measured HRR of microcapsules added in *n*-heptane/air combustion. (a) UF@PMP microcapsules addition; (b) PMMA@DMTP microcapsules addition. Small graphs inside indicate mHRR.

As depicted in Fig. 13, the addition of microcapsules in n-heptane results in a delayed TTI, and this delay increases with higher microcapsule concentrations. In comparison with the TTI of pure n-heptane, the TTI for *n*-heptane with 4% UF@PMP microcapsules was delayed by 56%. While increasing *n*-heptane from 4% to 8% showed no discernible effect on TTI, a 10% mass fraction led to a substantial 110% delay. Adding PMMA@DMTP microcapsules exhibited a similar trend, with a 10% additive amount causing a 120.7% delay in TTI. This observation suggests that a higher concentration of microcapsules can effectively mitigate the heat accumulation of combustible materials before ignition, facilitating search and rescue efforts and the evacuation of trapped individuals during a fire.

Although the addition of PMMA@DMTP microcapsules delays TTI, it has minimal impact on the pHRR of *n*-heptane. The pHRR for *n*-heptane with 10% PMMA@DMTP microcapsules closely resembles the pHRR of *n*-heptane without microcapsules during combustion. Conversely, the addition of UF@PMP microcapsules noticeably reduces pHRR. Combusting *n*-heptane with 4% UF@PMP microcapsules leads to a 15% decrease in pHRR, and at a 10% mass fraction, the pHRR drops by 27.8%, exceeding the experimental uncertainty. The distinction in the impact of the two microcapsules on HRR in the *n*-heptane combustion process is also evident in the modified heat-release rate (mHRR) shown in the inset of Fig. 13. During the combustion of *n*-heptane with 10% PMMA@DMTP microcapsules, mHRR decreases by 20.2% compared with n-heptane without microcapsules. Remarkably, achieving a comparable effect requires only 4% UF@PMP microcapsules (i.e., 20.6%). Further, at a 10% concentration, UF@PMP microcapsules result in a 35.1% reduction in mHRR, highlighting their superior efficacy in reducing the fire risk associated with fuel combustion.

3.4. Mechanism of microcapsules on fire safety enhancement of combustible materials

Fuel combustion involves the burning of gaseous substances produced by the fuel's evaporation or thermal decomposition [76].

The microcapsule thermal-response process comprises the vaporization release of the core material and the thermal decomposition of the wall material. By absorbing heat from the core material, along with the heat capacity and dilution of thermal decomposition gas products, the microcapsule can constrain fuel vaporization or evaporation time, as well as both mixing and induction times, thereby delaying the TTI.

As a typical fire-extinguishing agent, PMP can suppress flames through physical mechanisms and some chemical effects. Physical inhibition involves the high heat capacity of the gas mixture formed after PMP vaporization, extinguishing the through heat extraction-specifically, flame and fuel surface cooling [22,78]. On the other hand, chemical inhibition involves capturing flame-free radicals through pyrolysis and chain-termination reactions, converting them into stable components [78,79]. Initially, PMP decomposition follows two pathways: pyrolysis and the consumption of flame chain to transfer free radicals.

$$C_6F_{12}O \rightarrow C_2F_5CO + C_3F_7 \tag{4}$$

$$C_6F_{12}O + OH\bullet \rightarrow C_2F_5CO + C_3F_7OH \tag{5}$$

$$C_6F_{12}O + H\bullet \rightarrow C_2F_5CHO + C_3F_7 \tag{6}$$

$$C_6F_{12}O + O\bullet \rightarrow C_2F_5CO + C_3F_7O \tag{7}$$

The PMP consumption chain dominates the consumption process. In the chain-transfer process, CF_3CF_2, generated by the further decomposition of C_2F_5CO, is an essential intermediate component of pentafluoroethane (HFC-125), another inhibitor, in the inhibition reaction [80]. The formed C_2F_5 decomposes into effective inhibitory substances CF_2 and CF_3, essential chemical inhibitory components. Additionally, C_3F_7 is a significant component of heptafluoropropane (HFC-227ea), playing a role in chemical fire-extinguishing [81]. C_3F_7 combines with O free radicals to generate C_3F_7O and finally forms CF_3. C_2F_5, C_3F_7, CF_2, and CF_3 further react with the flame chain to transfer free radicals(O, H, and OH), generating stable substances, such as CF_2:O and HF. The main inhibitory reactions are as follows.

$$C_3F_7 + H\bullet \rightarrow C_3F_7H \tag{8}$$

$$C_3F_7 + O\bullet \rightarrow CF_3COF + CF_3 \tag{9}$$

$$CF_2 + OH\bullet \rightarrow CF:O + HF \tag{10}$$

$$CF_2 + O\bullet \rightarrow CF:O + F \tag{11}$$

$$CF_3 + H\bullet \rightarrow CF_2 + HF \tag{12}$$

$$CF_2:O + H\bullet \rightarrow CF:O + HF \tag{13}$$

As the core fire-extinguishing substance in both microcapsules, PMP participates in the chain reaction of *n*-heptane combustion, altering the chain-transfer mode. However, DMTP only exerts a physical heat absorption effect on flame inhibition [15]. Consequently, UF@PMP microcapsules can reduce the pHRR of the *n*-heptane flame, while PMMA@DMTP microcapsules have no significant effect on reducing pHRR.

The urea present in the wall material of UF@PMP microcapsules exhibits a fire-extinguishing effect. The inert CO_2 generated during thermal decomposition extinguishes fires through the turbulent effect induced by air dilution and volume expansion (approximately

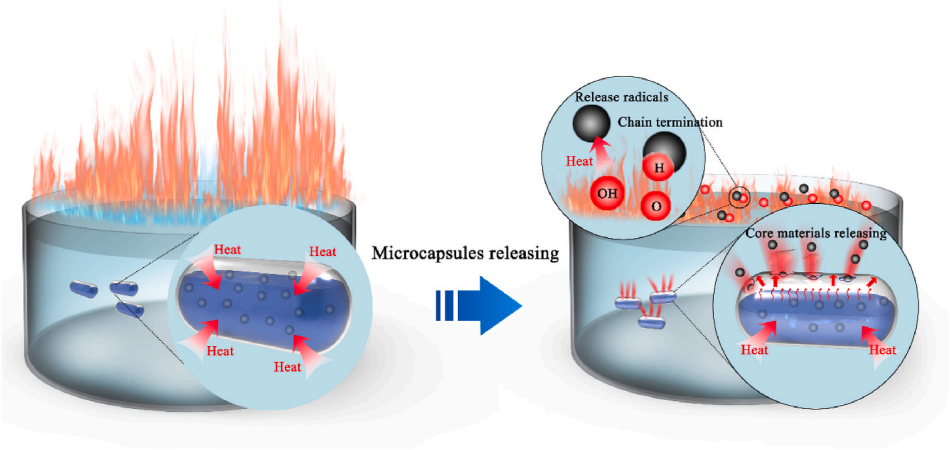

Fig. 14. Schematic of the fire-extinguishing mechanism of thermally responsive microcapsules.

1000 times [49]). Derek's research [82] demonstrated that a mixture of urea and potassium or sodium bicarbonate, carbonate and hydroxide exhibited high fire-extinguishing efficiency at 423K. Additionally, Zhou et al. [83] utilized urea as the primary component of multi-component additives to enhance the chemical fire-extinguishing efficiency of water mist. This turbulence effect, resulting from volume expansion, is observable in the lifting-off of the Cup burner flame, as depicted in Fig. 12 (b1) - (b6).

Conversely, the primary component of the wall material in PMMA@DMTP microcapsules, PMMA, is flammable. Upon reaching the pyrolysis temperature, solid polymethyl methacrylate converts into gaseous methyl methacrylate. This pyrolysis product contains various combustible components, including CO [84]. Consequently, UF@PMP microcapsules exhibit a superior flame-inhibition effect compared with PMMA@DMTP microcapsules.

In summary, the flame-inhibition mechanism of thermally responsive microcapsules involves a synergistic mechanism that integrates physical and chemical actions, as illustrated in Fig. 14.

In addition to CO_2, NH_3 is a thermal decomposition product of urea when water vapor is present in the combustion products, as shown in Formula (14).

$$CO(NH_2)_2 + H_2O \xrightarrow{>433K} 2NH_3 + CO_2 \tag{14}$$

The presence of NH_3 as a combustible substance, introduces a partial weakening of the inhibitory effect of urea on the flame. According to Joseph et al. [48], the application of urea as an additive tends to prolong the fire-extinguishing time, as observed in research on the fire-extinguishing efficiency of water mist with additives. Simultaneously, formaldehyde, another significant component in the wall material of UF@PMP microcapsules, is also combustible, impacting the overall fire-extinguishing effectiveness. Consequently, the efficacy of the two microcapsules in this study concerning flame suppression is contingent upon the interplay between the promoting effect of some thermal decomposition products from the wall material and the inhibitory effect of the core material. At lower concentrations of microcapsules, the promoting effect remains significant, even though the inhibitory effect is dominant. This results in an indistinct reduction in MEC and mHRR as the microcapsule concentration increases from 2% to 8%. Upon surpassing a critical threshold (i.e., 10%), the microcapsules effectively inhibit the target flame, counteracting the combustion promotion caused by the thermal decomposition of the wall material. Notably, the microcapsules can even achieve self-extinguishing (i.e., 14.5% in the self-extinguishing test) without additional fire-extinguishing agents, owing to the substantial excess of core materials over wall materials. Subsequently, the inhibitory effect of microcapsules on the flame experiences a noteworthy enhancement. Due to UF@PMP microcapsules possessing more capabilities than PMMA@DMTP microcapsules, the additional mass has a more pronounced impact on the inhibitory role of UF@PMP microcapsules compared with PMMA@DMTP microcapsules.

The law of energy conservation serves as the theoretical foundation for extinguishing agents in inhibiting and extinguishing flames. The energy absorbed by the fire-extinguishing agent through various action mechanisms consistently exceeds the energy released by the flame. However, the released energy of the flame lies within a range rather than being a fixed value. In a prior study [85], the fire-extinguishing agent obtained through the Cup-burner test exhibited upper and lower limits in MEC, corresponding to the lower and upper bounds of energy released in the experimental flame. The input amount of microcapsules under various working conditions is a constant value (i.e., the absorbed energy remains relatively stable). When the additional amount is low, an increase in mass fraction does not lead to a significant improvement in the absorbed energy if it falls within the range of the energy released by the flame.

This study has a few limitations. First, the limited number of reported studies on this subject necessitated an exploratory approach. The availability of experimental samples was constrained, potentially impacting the verification of fire-extinguishing performance utilizing microcapsules. Second, the equipment employed to validate the proposed method was limited, thereby influencing the accuracy of our results. For example, FESEM analysis was conducted solely on one type of microcapsules (i.e., UF@PMP microcapsules), the composition of residue materials post the interaction between microcapsules and flame was not documented, and aspects such as the relative toxicity of smoke and other gaseous components during the interaction of microcapsules with the flame were not recorded. These compromises were necessitated by limitations in time and funding. Simultaneously, several avenues for future research could be explored based on the current study's limitations. First, microcapsules were incorporated into diverse materials and coatings to enhance their fire-extinguishing properties, characterized by uniform analytical methods. Second, when evaluating comprehensive fire-extinguishing performances, considerations should extend beyond only fire-extinguishing time and the suppression of associated thermal hazards. It is imperative to assess the suppression of smoke and gaseous hazards. Consequently, synchronous inclusion of testing equipment for smoke and gaseous components is recommended in fire-extinguishing tests.

4. Conclusions

(1) Under appropriate conditions, PMP can undergo microencapsulation using UF as a wall material through in-situ polymerization. UF demonstrates a thermal insulation effect, raising the phase-transition temperature of microencapsulated PMP from 49 °C to 120 °C.

(2) DMTP can be microencapsulated via solvent evaporation with PMMA as a wall material under suitable conditions. Moreover, the response temperature for DMTP microencapsulation spans from 88 °C to 95 °C.

(3) The encapsulation rate of microcapsules is intricately linked to the preparation method and the selection of core and wall materials. In this study, UF @ PMP microcapsules achieved an encapsulation rate of 70 %, while PMMA @ DMTP microcapsules reached approximately 50 %.

(4) Fuel containing additional UF @ PMP and PMMA @ DMTP microcapsules could self-extinguish during combustion. When the fluoride solution of the core material attains the threshold temperature, the gas pressure generated in the vaporization-phase change can breach the shell, releasing gas for active fire protection.
(5) In scenarios where the extra UF @ PMP and PMMA @ DMTP microcapsules in the fuel fail to achieve self-extinguishing, enhancing the material's fire-resistant performance is possible by reducing the quantity of fire-extinguishing agents in the extinguishing process. This involves delaying the ignition time of the fuel and diminishing the HRR during combustion. Furthermore, the degree of improvement is strongly correlated with the additional amount, as well as the type of wall and core materials in the microcapsules.
(6) The mechanism of UF @ PMP microcapsules in enhancing the fire-resistant performance of materials incorporates a comprehensive blend of physical and chemical effects. It demonstrates a more effective improvement compared with PMMA @ DMTP microcapsules, which operate with a single physical mechanism.

Data availability statement

Data will be made available on request.

CRediT authorship contribution statement

Hao Liu: Writing – review & editing, Funding acquisition, Data curation. **Tianwei Zhang:** Methodology, Investigation, Funding acquisition. **Man Zhang:** Writing – review & editing, Methodology, Funding acquisition. **Cunwei Zhang:** Methodology. **Zidong Guo:** Funding acquisition, Data curation. **Yuhai Zhang:** Funding acquisition. **Haoran Chen:** Investigation, Funding acquisition. **Yunchen Wu:** Methodology. **Guiyun Zhang:** Methodology.

Declaration of competing interest

The authors declare that they have no known competing financial interests or personal relationships that could have appeared to influence the work reported in this paper.

Acknowledgement

Financial support was provided by the Natural Science Foundation of Hebei Province (E2023507001), the Open Fund of Hebei Key Laboratory of Hazardous Chemicals Safety and Control Technology (20211204-4), the Key R&D Program of Hebei Province (22375417D), the Science and Technology Program of Fire and Rescue Department Ministry of Emergency Management (2022XFCX19) and the National Natural Science Foundation of China (51804314).

References

[1] Y. Quan, Z. Zhang, R. Tanchak, et al., A review on cone calorimeter for assessment of flame-retarded polymer composites[J], J. Therm. Anal. Calorim. 147 (19) (2022) 10209–10234.
[2] Z. Zhang, Q. Xie, M. Ren, et al., Pyrolysis and thermal behavior of unginned cotton piles: effects of mildewing and impurities[J], J. Therm. Anal. Calorim. 147 (1) (2022) 123–134.
[3] Y. Luo, Q. Li, L. Jiang, et al., Analysis of Chinese fire statistics during the period 1997-2017[J], Fire Saf. J. 125 (2021) 103400.
[4] M. Rohilla, A. Saxena, Y. Tyagi, et al., Condensed aerosol based fire extinguishing system covering versatile applications: a review[J], Fire Technol. 58 (1) (2022) 327–351.
[5] M. Mahbub, M. Hossain, M. Gazi, Cloud-enabled loT-based embedded system and software for intelligent indoor lighting, ventilation, early stage fire detection and prevention[J], Comput. Network. 184 (2021) 107673.
[6] J.X. Wang, Q. Yu, X. Zhao, Pyrolysis characters and fire behavior of bus ceiling materials[J], J. Therm. Anal. Calorim. 146 (4) (2021) 1641–1656.
[7] M. Mahbub, M. Hossain, M. Gazi, Cloud-enabled loT-based embedded system and software for intelligent indoor lighting, ventilation, early stage fire detection and prevention[J], Comput. Network. 184 (2021) 10773.
[8] Y. Zeng, H. Wong, W. Wegrzynski, et al., Revisiting Alpert's correlations: numerical exploration of early-stage building fire and detection[J], Fire Technol. 59 (5) (2023) 2925–2948.
[9] A. Vasiliev, A. Varfolomeev, I. Volkov, et al., Reducing humidity response of gas sensors for medical applications: use of spark discharge synthesis of metal oxide nanoparticles[J], Sensors 18 (8) (2018) 2600.
[10] X. Li, A. Vazquez-Lopez, J. Saez, et al., Recent advances on early-stage fire-warning systems: mechanism, performance, and perspective[J], Nano-Micro Lett. 14 (1) (2022) 226.
[11] H. Liu, X. Wang, D. Wu, et al., Fabrication and applications of dual-responsive microencapsulated phase change material with enhanced solar energy-storage and solar photocatalytic effectiveness[J], Sol. Energy Mater. Sol. Cell. 193 (2019) 184–197.
[12] H. Liu, Z. Han, Q. Wang, et al., Surface construction of $Ni(OH)_2$ nanoflowers on phase-change microcapsules for enhancement of transfer and thermal response [J], Appl. Surf. Sci. 562 (2021) 150211.
[13] C. Yu, J. Joun, Y. Song, Encapsulated phase change material embedded by graphene powders for smart and flexible thermal response[J], Fibers Polym. 20 (3) (2019) 545–554.
[14] L. Zhao, N. Sottos, Autonomous strategies for improved performance and reliability of Li-ion batteries, Adv. Energy Mater. 11 (5) (2021) 2003139.
[15] T. Yim, M. Park, S. Woo, et al., Self-extinguishing lithium ion batteries based on internally embedded fire-extinguishing microcapsules with temperature-responsiveness[J], Nano Lett. 15 (8) (2015) 5059–5067.
[16] C. Chen, C. Li, Microencapsulating inorganic and organic flame retardants for the safe improvement of lithium-ion batteries, Solid State Ionics 323 (2018) 56–63.
[17] M. Baginska, N. Sottos, S. White, Core-shell microcapsules containing flame retardant tris(2-chloroethyl phosphate) for lithium-ion battery applications[J], ACS Omega 3 (2018) 1609–1613.

[18] B. Kazanci, K. Cellat, H. Paksoy, Preparation, characterization, and thermal properties of novel fire-resistant microencapsulated phase change materials based on paraffin and a polystyrene shell[J], RSC Adv. 10 (40) (2020) 24134–24144.
[19] H. Xing, S. Lu, H. Yang, et al., Review on research progress of $C_6F_{12}O$ as a fire extinguishing agent[J], Fire-Switzerland 5 (2) (2022) 50.
[20] T. Zhang, H. Liu, J. Song, et al., Synergistic inhibition effect on lithium-ion batteries during thermal runaway by N_2-twin-fluid liquid mist[J], Case Stud. Therm. Eng. 37 (2022) 102269.
[21] J. Pagliaro, G. Linteris, P. Sunderland, et al., Combustion inhibition and enhancement of premixed methane-air flames by halon replacement[J], Combust. Flame 162 (1) (2015) 41–49.
[22] Available from:, 3M^{TM} Novec^{TM} 1230 Fire Protection Fluid Technical Data, 2020 https://multimedia.3m.com/mws/media/124688O/3m-novec-1230-fire-protection-fluid.pdf. Last checked: August 3.
[23] A. Vilesov, O. Suvorova, V. Yudin, et al., Novel microencapsulated liquid fire extinguishers with a nanomodified microcapsule shell[J], Polym. Sci. B 56 (4) (2014) 512–519.
[24] A.D. Vilesov, N.N. Saprykina, R.V. Stepanov, et al., Microencapsulated fire-extinguishing fluids and reactive fire-extinguishing composites formed on their basis [J], Polym. Sci. 54 (6) (2012) 499–504.
[25] D.H. Lee, S. Kwon, Y.E. Kim, et al., Double-layered polymer microcapsule containing non-flammable agent for initial fire suppression[J], Materials 15 (21) (2022) 7831.
[26] W. Zhang, L. Wu, J. Du, et al., Fabrication of a microcapsule extinguishing agent with a core-shell structure for lithium-ion battery fire safety[J], Mater. Adv. 2 (14) (2021) 4634–4642.
[27] Y. Yang, X.F. Wang, M.Y. Pan, et al., Evaluation on algorithm reliability and efficiency for an image flame detection technology[J], J. Therm. Anal. Calorim. (2023) (Early Access).
[28] Y.C. Liu, J.C. Jiang, A.C. Huang, Experimental study on extinguishing oil fire by water mist with polymer composite additives[J], in: Journal of Thermal Analysis and Calorimetry,, 2022 (Early Access).
[29] A.C. Huang, F.C. Liao, C.F. Huang, et al., Calorimetric approach to establishing thermokinetics for cosmeceutical benzoyl peroxides containing metal ions[J], J. Therm. Anal. Calorim. 144 (2) (2021) 373–382.
[30] Y.C. Liu, H.L. Zhou, Y. Tang, et al., Thermal hazard assessment by TGA, DSC, and ARC experimental and simulated thermokinetic approaches for trinitrophloroglucinol[J], in: Journal of Thermal Analysis and Calorimetry, 2022 (Early Access).
[31] Z.P. Li, A.C. Huang, Y. Tang, et al., Thermokinetic prediction and safety evaluation for toluene sulfonation process and product using calorimetric technology [J], J. Therm. Anal. Calorim. 147 (21) (2021) 12177–12186.
[32] Y. Tang, Z.P. Li, H.L. Zhou, et al., Thermal stability assessment of nitrocellulose by using multiple calorimetric techniques and advanced thermokinetics, in: Journal of Thermal Analysis and Calorimetry, 2022 (Early Access).
[33] H. Wu, J.C. Jiang, A.C. Huang, et al., Effect of emulsifiers on the thermal stability of firework propellants[J], in: Journal of Thermal Analysis and Calorimetry, 2022 (Early Access).
[34] Y.C. Liu, A.C. Huang, Y. Tang, et al., Thermokinetic analysis of the stability of acetic anhydride hydrolysis in isothermal calorimetry techniques[J], J. Therm. Anal. Calorim. 147 (14) (2022) 7865–7873.
[35] F.H. Chen, G.H. Wen, P. Tang, et al., The role of carbonaceous materials in mold powder and influence on melting behavior[J], J. Therm. Anal. Calorim. 147 (20) (2022) 10965–10975.
[36] J.G. Yang, L.H. Luo, J. Gao, et al., Study on the effect of regeneration agent on the viscosity properties of aged asphalt[J], Materials 15 (1) (2022) 380.
[37] W.W. Duan, Z.J. Zhang, J.J. Zhu, et al., Comparative analysis of the phenolic profile of lyceum barbarum L. fruits from different regions in China[J], Molecules 27 (18) (2022) 5842.
[38] H.L. Zhou, J.C. Jiang, A.C. Huang, et al., Calorimetric evaluation of thermal stability and runaway hazard based on thermokinetic parameters of O,O-dimethyl phosphoramidothioate[J], J. Loss Prev. Process. Ind. 75 (2022) 104697.
[39] A.C. Huang, C.F. Huang, Y. Tang, et al., Evaluation of multiple reactions in dilute benzoyl peroxide concentrations with additives using calorimetric technology [J], J. Loss Prev. Process. Ind. 69 (2021) 104373.
[40] A.C. Huang, C.F. Huang, Z.X. Xing, et al., Thermal hazard assessment of the thermal stability of acne cosmeceutical therapy using advanced calorimetry technology[J], Process Saf. Environ. Protect. 131 (2019) 197–204.
[41] T. Yim, M.S. Park, S.G. Woo, et al., Self-extinguishing lithium-ion batteries based on internally embedded fire extinguishing microcapsules with temperature-responsiveness[J], Nano Lett. 15 (8) (2015) 5059–5067.
[42] J.H. Wang, Y. Yamada, K. Sodeyama, et al., Fire-extinguishing organic electrolytes for safe batteries[J], Nat. Energy 3 (1) (2018) 22–29.
[43] D. Zhou, Y.B. He, R.L. Liu, et al., In situ synthesis of a hierarchical all-solid-state electrolyte based on nitrile materials for high-performance lithium-ion batteries [J], Adv. Energy Mater. 5 (15) (2015) 1500353.
[44] Z.Y. Han, R.C. Zi, Y. Yu, et al., Study on the minimum extinguishing concentration of $C_6F_{12}O$ for extinguishing synthesis gas flame of lithium-ion battery[J], J. Therm. Anal. Calorim. 148 (9) (2023) 3631–3643.
[45] J.C. Zhao, Y.Y. Fu, S. Lu, et al., An improved method to determine the minimum extinguishing concentration of ultrafine dry powder agents: taking $NaHCO_3$ and $KHCO_3$ as examples, Process Saf. Environ. Protect. 172 (2023) 846–856.
[46] Y. Koshiba, Y. Hirakawa, Fire-suppression Efficiency and Extinguishing Mechanisms of Calcium Acetate Using Heptane Cup-Burner flames[J]. Fire and Materials, Early Access, 2023.
[47] Z.Q. Chen, W. Xu, Y. Jiang, Investigation of the effect of dimethyl methylphosphonate (DMMP) on flame extinction limit of lithium-ion battery electrolyte solvents[J], Fuel 270 (2020) 117423.
[48] P. Joseph, E. Nichols, V. Noyozhilov, A comparative study of the effects of chemical additives on the suppression efficiency of water mist, Fire Saf. J. 58 (2013) 221–225.
[49] T.S. Liang, R.W. Li, J. Li, et al., Extinguishment of hydrocarbon pool fires by ultrafine water mist with ammonium/amidogen compound in an improved cup burner[J], Fire Mater. 42 (8) (2018) 889–896.
[50] Y.L. Zhao, X.L. Zhang, S.F. Luo, et al., Effect of oxygen concentration and external radiation on the thermal decomposition and combustion characteristics of electric wire[J] 147 (14) (2022) 7775–7784.
[51] J. Chen, X.L. Zhang, Y.L. Zhao, et al., Oxygen concentration effects on the burning behavior of small-scale pool fires[J], Fuel 247 (2019) 378–385.
[52] ASTM E.2058-00:standard test method for measurement of synthetic polymer material flammability using a fire propagation apparatus(FPA), Am. Soc. Test Mater. 100 (2000).
[53] S. Brohez, C. Delvosalle, G. Marlair, The measurement of heat release from oxygen consumption in sooty fires[J], J. Fire Sci. 18 (5) (2000) 327–353.
[54] B.D. Ditch, J.L. de Ris, T.K. Blanchat, et al., Pool fires – an empirical correlation[J], Combust. Flame 160 (12) (2013) 2964–2974.
[55] S. Xu, H. Xiao, Y. Chen, et al., Preparation and thermal degradation property analysis of the tea-based melamine-modified urea-formaldehyde(TMUF) resin, J. Therm. Anal. Calorim. 146 (4) (2021) 1845–1852.
[56] B. Grabowska, S. Zymankowska-Kumon, S. Cukrowicz, et al., Thermoanalytical tests(TG-DTG-DSC, Py-GC/MS) of foundry binders on the example of polymer composition of poly(acrylic acid)-sodium carboxymethylcellulose, J. Therm. Anal. Calorim. 138 (6) (2019) 4427–4436.
[57] X. Shan, J. Wang, X. Zhang, et al., Formaldehyde-free and thermal resistant microcapsules containing n-octadecane, Thermochim. Acta 494 (1–2) (2009) 104–109.
[58] Z. Lin, X. Wang, Nanostructure engineering and doping of conjugated carbon nitride semiconductors for hydrogen photosynthesis, Angew. Chem. Int. Ed. 52 (6) (2013) 1735–1738.
[59] G. Vazquez, F. Lopez-Suevos, A. Villar-Garea, et al., C-13-NMR analysis of phenol-urea-formaldehyde prepolymers and phenol-urea-formaldehyde-tannin adhesives[J], J. Adhes. Sci. Technol. 18 (13) (2004) 1529–1543.

[60] A. Kandelbauer, A. Despres, A. Pizzi, et al., Testing by fourier transform infrared species variation during melamine-urea-formaldehyde resin preparation[J], J. Appl. Polym. Sci. 106 (4) (2007) 2192–2197.
[61] S. Kavukcu, S. Gunnaz, O. Sahin, et al., Piano-stool Ru(II) arene complexes that contain ethylenediamine and application in alpha-alkylation reaction of ketones with alcohols[J], Appl. Organomet. Chem. 33 (5) (2019) e4888.
[62] R. Ebewele, G. Myers, B. River, et al., Polyamine-modified urea-formaldehyde resins.1.Systhesis, structure, and properties[J], J. Appl. Polym. Sci. 42 (11) (1991) 2997–3012.
[63] K. Behler, M. Havel, Y. Gogotsi, New solvent for polyamides and its application to the electrospinning of polyamides 11 and 12[J], Polymer 48 (22) (2007) 6617–6621.
[64] G. Sui, W. Zhong, X. Yang, et al., Preparation and properties of nature rubber composites reinforced with pretreated carbon nanotubes[J], Polym. Adv. Technol. 19 (11) (2008) 1543–1549.
[65] N. Sahan, D. Nigon, S. Mantell, et al., Encapsulation of stearic acid with different PMMA-hybrid shell materials for thermotropic materials[J], Sol. Energy 184 (2019) 466–476.
[66] T. Pal, S. Paul, B. Sa, Polymethylmethacrylate coated alginate matrix microcapsules for controlled release of diclofenac sodium[J], Pharmacol. Pharm. 2 (2) (2011) 56–66.
[67] W. Zeng, S. Li, W. Chow, Review on chemical reactions of burning Poly(methyl methacrylate)PMMA[J], J. Fire Sci. 20 (5) (2002) 401–433.
[68] U. Ali, K. Karim, N.A. Buang, A review of the properties and applications of poly (methyl methacrylate) (PMMA)[J], Polym. Rev. 55 (4) (2015) 1–28.
[69] T. Zhang, X. Liu, G. Wang, et al., Sustained effect of dry water in thermal environment after fire extinguishing: fuel surface coating methods[J], Case Stud. Therm. Eng. 27 (2021) 101237.
[70] E. Zegers, B. Williams, E. Fisher, et al., Suppression of nonpremixed flames by fluorinated ethanes and propanes[J], Combust. Flame 121 (3) (2000) 471–487.
[71] N. Saito, Y. Ogawa, Y. Saso, et al., Flame-extinguishing concentrations and peak concentrations of N_2, Ar, CO_2 and their mixtures for hydrocarbon fuels, Fire Saf. J. 27 (1996) 185–200.
[72] T. Moore, C. Weitz, R. Tapscott, An update on NMERI cup-burner test results[C]. Halon Options technical Working Conference, Proceedings (1996) 551–564.
[73] ISO 14520 Part 1, Gaseous Fire-Extinguishing Systems-Physical Properties and System Design, International Organization for Standardization, 2000.
[74] S. Zhang, M. Colket, Modelling cup-burner minimum extinguishing concentration of halogenated agent[J], Proc. Combust. Inst. 33 (2011) 2497–2504.
[75] J. Gilman, C. Jackson, A. Morgan, et al., Flammability properties of polymer-layered-silicate nanocomposites. Polypropylene and polystyrene nanocomposites, Chem. Mater. 12 (7) (2000) 1866–1873.
[76] Y. Roman-Leshkov, C. Barrett, Z. Liu, et al., Production of dimethylfuran for liquid fuels from biomass-derived carbohydrates[J], Nature 447 (7147) (2007), 982-U5.
[77] J. Quintiere, A simplified theory for generalizing results from a radiant panel rate of flame spread apparatus[J], Fire Mater. 5 (2) (1981) 52–60.
[78] W. Xu, Y. Jiang, X. Ren, Combustion promotion and extinction of premixed counterflow methane/air flames by $C_6F_{12}O$ fire suppressant[J], J. Fire Sci. 34 (4) (2016) 289–304.
[79] L. Liu, Z. Du, T. Zhang, et al., The inhibition/promotion effect of $C_6F_{12}O$ added to a lithium-ion cell syngas premixed flame[J], Int. J. Hydrogen Energy 44 (39) (2019) 22282–22300.
[80] W. Xu, Y. Jiang, R. Qiu, et al., Influence of halon replacements on laminar flame speeds and extinction limits of hydrocarbon flames[J], Combust. Flame 182 (2017) 1–13.
[81] J. Xu, P. Guo, Q. Duan, et al., Experimental study of the effectiveness of three kinds of extinguishing agents on suppressing lithium-ion battery fires[J], Appl. Therm. Eng. 171 (2020) 115076.
[82] B.J. Derek, Fire-extinguishing compositions comprising the reaction products of urea and a bicarbonate, carbonate or hydroxide of sodium or potassium, U.S. Patent 3 (530) (1970), 620, Oct. 27,.
[83] X. Zhou, G. Liao, C. Bo, Improvement of water mist's fire-extinguishing efficiency with MC additive[J], Fire Saf. J. 41 (2006) 39–45.
[84] M. Ferriol, A. Gentilhomme, M. Cochez, et al., Thermal degradation of poly (methyl methacrylate)(PMMA): modelling of DTG and TG curves[J], Polym. Degrad. Stabil. 79 (2) (2003) 271–281.
[85] T. Zhang, H. Liu, Z. Han, Active substances study in fire extinguishing by water mist with potassium salt additives based on thermoanalysis and thermodynamics [J], Appl. Therm. Eng. 122 (2017) 429–438.